Tokamak ion temperature and poloidal field diagnostics using 3-MeV protons

W. W. Heidbrink and J. D. Strachan

Plasma Physics Laboratory, Princeton University, Princeton, New Jersey 08544

(Received 27 August 1984; accepted for publication 3 January 1985)

The 3-MeV protons created by $d(d, p)t$ fusion reactions in a moderately sized tokamak leave the plasma on trajectories determined by the position of their birth and by the poloidal magnetic field. Pitch-angle resolution of the escaping 3-MeV protons can separately resolve the spatial distribution of the $d(d, p)t$ fusion reactions and the poloidal field distribution inside the tokamak. These diagnostic techniques have been demonstrated on PLT with an array of collimated surface barrier detectors.

INTRODUCTION

The internal structure of the magnetic field is a fundamental property of a magnetic confinement device. Because of its importance in achieving an understanding of the stability and energy balance of tokamak plasmas, development of diagnostic methods to measure the poloidal field is an active line of research.[1] Methods include magnetic probes on small machines, Faraday rotation measurements,[2–4] measurements of the Zeeman splitting of injected lithium,[5] wave scattering off gyrating electrons,[6] measurements of the toroidal displacement of an injected heavy ion beam,[1] and measurements of the orbit shift of high-energy ions injected with a diagnostic neutral beam.[7] Less direct techniques include studies of the effect of current fluctuations on Alfvén wave propagation,[8] measurements of the mode structure and spatial distribution of oscillations in the soft x-ray emission (or another emission), which are then taken to be the $q = 1$ or $q = 2$ surface,[9] the ratio of equilibrium field to plasma current, which, in MHD theory, is related to the plasma inductance,[10] and measurements of the electron temperature profile, which are then related to the plasma current using the theoretical dependence of the plasma resistivity on electron temperature and the assumptions of a uniform impurity content and toroidal electric field.[1]

The ion temperature profile is a second fundamental property of a tokamak plasma that is necessary for evaluation of plasma heating and transport. Although measurements of the central ion temperature frequently are made using charge-exchanged neutrals,[11] neutrons,[12] and Doppler broadening of impurity x-ray lines,[13] ion temperature profiles are less common. Techniques include spectroscopic measurements of the Doppler broadening of visible atomic transitions from injected impurities[14] or from helium transitions excited by a diagnostic neutral beam,[15] and detection of the charge-exchange efflux from a diagnostic neutral beam.[16] Another possible technique is to measure the spatial distribution of $d(d, n)^3$He fusion reactions (which is related to the ion temperature profile in a thermal plasma) but, because of difficulties in adequately collimating the 2.4-MeV neutron detectors to reject scattered neutrons, previous workers[17,18] were unable to measure the fusion emissivity in regions of the plasma with $\lesssim 10\%$ of the maximum value of the emissivity, so this diagnostic technique has not yielded an accurate temperature profile.

This paper discusses new methods of measuring the tokamak poloidal field and ion temperature profile based on measurements of 3-MeV protons created in $d(d, p)t$ fusion reactions. In a tokamak, most fusion reactions take place near the center of the device where the plasma is hottest and most dense. In a machine the size of the PLT tokamak, a large fraction of the 3-MeV protons born near the center of the plasma escape the plasma on orbits that eventually intersect the vacuum vessel wall. Near the vessel wall, the protons can be measured using silicon surface barrier detectors.[19] The proton flux and angle of incidence at the detector are determined by the spatial distribution of the fusion reactions that produce the protons and by the magnetic field, which governs the orbits of the protons. For measurements of the emission profile, the detector orientations and positions are selected to minimize the sensitivity of the flux to the tokamak magnetic fields. Because charged particles scatter much less than neutrons, excellent collimation is readily achieved and accurate measurements of the emissivity in regions with $\lesssim 1\%$ of the peak emissivity are possible. For poloidal field measurements, the detectors are oriented to measure protons on orbits close to "stagnation orbits"[20] in order to maximize the sensitivity of the proton flux to the poloidal field. Measurements in the region $0.2 \lesssim r/a \lesssim 0.6$ accurate to 5% might be possible.

The paper is organized as follows. In Sec. I, optimal detector orientations for measurements of the fusion emission profile and of the poloidal field are presented. Section II introduces the concept of proton detection efficiency, which is used to relate the proton flux measured by a detector to proton orbits in the plasma. Included in this section are measurements of the collimation properties of seven detectors used to test these diagnostic techniques on PLT. Next, sample data from the PLT experiment are described (Sec. III). The paper concludes with an assessment of proton ion temperature and poloidal field diagnostics relative to other diagnostic techniques (Sec. IV).

I. PROTON ORBITS

The orbit of an ion in a magnetic field that is slowly varying in space and time can be decomposed into three types of motion: a fast circular gyromotion perpendicular to the magnetic field, a "free-streaming" motion parallel to the

 0034-6748/85/040501-18$01.30

field lines, and a set of slow drifts perpendicular to the field lines. Even though fusion product orbits are large compared to the minor radius a of the tokamak, the analysis of these orbits in terms of guiding-center drifts is usually valid. The criterion for the validity of guiding-center theory is that $\rho/L \lesssim 0.2$, where ρ is the ion gyroradius and L is the scale length of magnetic field inhomogeneity. Because of the large toroidal field in a tokamak, the proper value to select for the scale length of field variations is the tokamak major radius R; for 3-MeV protons in PLT this yields a ratio of $\rho/L \lesssim 10\,\text{cm}/140\,\text{cm} = 0.07$, so the criterion for guiding-center theory is well satisfied. It should be noted, however, that ρ is *not* small compared to the plasma minor radius a, so for calculations of the position of a particle it is a poor approximation to follow its guiding center.

In a tokamak, the magnetic field in the toroidal direction is an order of magnitude larger than the field in the poloidal direction, so the trajectory of ions is dominated by the topology of the toroidal field. The circular gyromotion is primarily in the plane perpendicular to the toroidal field, the free-streaming motion is primarily in the toroidal direction, and the direction of the perpendicular drifts is determined by the inhomogeneity of the toroidal magnetic field. When projected onto a poloidal plane, the ion trajectory consists of circular gyromotion superimposed on a slow "drift orbit" consisting of the poloidal component of the free-streaming motion

$$v_\theta \simeq v_\parallel B_\theta / B_\phi \tag{1}$$

and the vertical drift motion

$$v_d = v_{\nabla B} + v_{\text{curvature}} \simeq (\tfrac{1}{2} v_\perp^2 + v_\parallel^2)/\Omega R, \tag{2}$$

where $v_\perp$ and $v_\parallel$ are the ion velocities perpendicular and parallel to the field lines, respectively, and Ω is the (local) ion gyrofrequency. In addition to these components of the motion, there also are drifts associated with electric fields, with toroidal field ripple, with plasma instabilities, and with stray fields but, for unconfined MeV ions, these drifts are estimated to be an order of magnitude weaker than the poloidal free-streaming [Eq. (1)] and vertical drift [Eq. (2)] motions. Because both drift motions v_θ and v_d depend inversely on the magnitude of the toroidal field B_ϕ, changes in toroidal field do not affect the shape of the ion drift orbit. Changes in toroidal field act only to alter the rate at which the drift orbit is traversed and the radius and frequency of gyromotion about that drift orbit. Changes in poloidal field B_θ change the shape of the ion drift orbit by modifying the free-streaming contribution to the motion [Eq. (1)] without affecting the vertical drift motion [Eq. (2)].

There is a class of orbits that is insensitive to changes in poloidal field, however, and it is these orbits that are selected to measure the emission profile. For particles without parallel velocity, the free-streaming contribution to the motion vanishes [Eq. (1)] and the ion drift orbit consists of the vertical ∇B drift alone. The optimal configuration of an array of detectors intended to measure the emission profile consists of several detectors at several poloidal positions along the vacuum vessel wall, each of which is oriented to measure protons that have no parallel velocity near the midplane (Fig. 1).

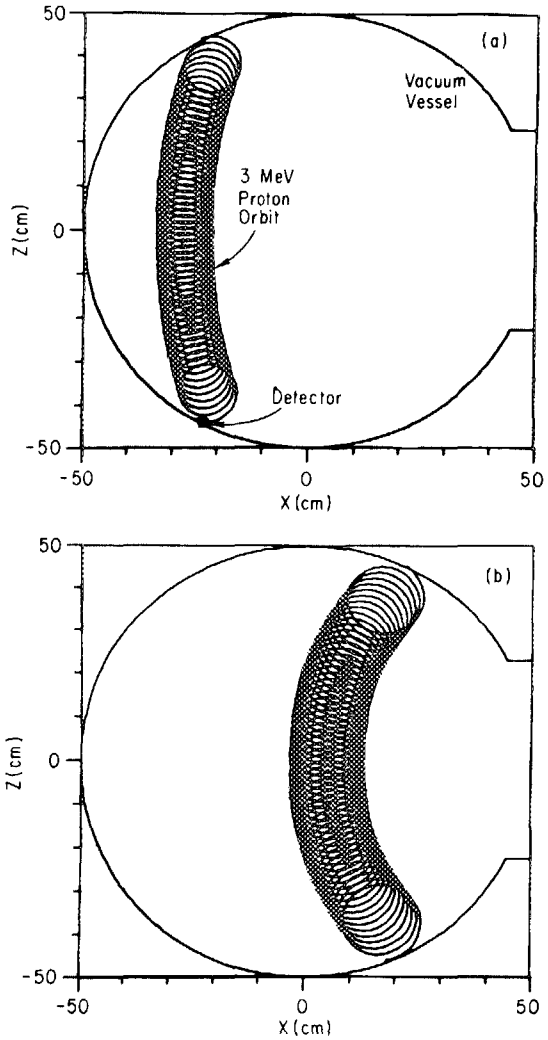

FIG. 1. Poloidal projection of 3-MeV proton orbits in PLT ($a = 40$ cm; $R_0 = 132$ cm; $B_\phi = 32$ kG; $I_\phi = 430$ kA; $j \propto [1 - (r/a)^2]^4$). The position and velocity of the protons at the detector are (a) $R = 107$ cm, $z = -43$ cm, $\sin v_\phi/v = 0.31$; (b) $R = 150$ cm, $z = -46$ cm, $\sin v_\phi/v = 0.36$; where $v_\phi \equiv \hat{\phi}\cdot\mathbf{v}/v$. Measurements of orbits like these with a poloidal array of collimated proton detectors yields the profile of $d\,(d, p)t$ fusion reactions.

Protons with no parallel velocity near the midplane do have some parallel velocity near the detector. The proton orbits selected for emission profile measurements are large unconfined orbits that can be thought of as cocirculating orbits with little parallel velocity or as banana-trapped orbits with the turning point at the midplane. The 3-MeV protons are well suited for emission profile measurements in PLT because they are poorly confined in the appropriate part of velocity space while the particle gyroradius is about 1/5 of the plasma radius. On a smaller device, detection of the 0.8-MeV ^{3}He ion might be more suitable for emission profile measurements. On a larger device such as TFTR, 15-MeV protons have orbits similar to 3-MeV proton orbits on PLT, so that measurement of the $d\,(^3\text{He}, p)\alpha$ emission profile is possible. It also appears feasible to use 3.7-MeV alphas to measure the $d\,(^3\text{He}, \alpha)p$ emission profile on a tokamak the size of PLT.[21]

An array of emission profile detectors (Fig. 1) can be thought of as a set of vertical chords looking up through the plasma. For a flat emission profile, the spatial resolution of

one of these detectors is about 15 cm since the detector measures any protons produced in a swath that is a proton gyrodiameter wide ($\sim$15 cm at 32 kG). In practice, however, the emission profile peaks strongly near the magnetic axis so that the flux measured by a given detector is dominated by the portion of the orbit closest to the plasma center and the spatial resolution can be a few centimeters.

The above discussion can be made more quantitative. The signal actually measured by a proton detector is proportional to the emission-weighted length of the proton orbit $\int S\,dl$ (Sec. II), where S is the fusion emissivity. Calculating the quantity $\int S\,dl$ using a wide range of model poloidal fields indicates that the detection efficiency for an array of detectors oriented to measure protons with no parallel velocity near the midplane is indeed quite insensitive to the distribution of the plasma current [Fig. 2(a)]. In contrast, the signal is predicted to depend strongly on the emission profile [Fig. 2(b)]. The physical explanation for Fig. 2(b) is that the flux measured by a detector that looks through the center of the plasma is reduced for broader emission profiles but the flux

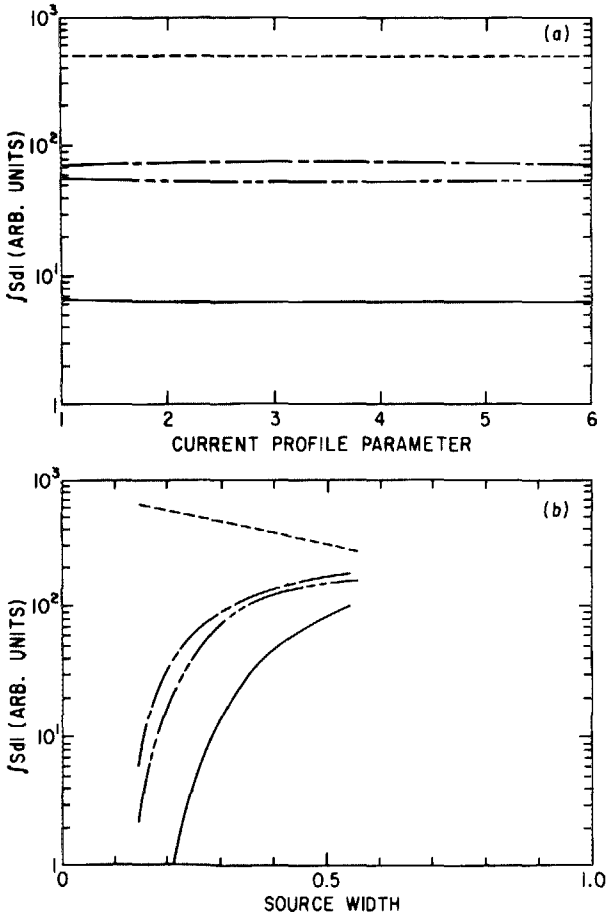

FIG. 2. (a) Emission-weighted orbit length $\int S\,dl$ vs the breadth of the plasma current profile for emission profile detectors at $R = 107$ cm (solid line), $R = 118$ cm (short-short-long dash), $R = 150$ cm (short dash), and $R = 166$ cm (short-long dash). The current is assumed of the form $j \propto [1 - (r/a)^2]^i$, where i is the current profile parameter. A fairly broad thermonuclear profile $\{S(r) \propto [1 - (r/a)^2]^9\}$ was used in the calculation. (b) Normalized emission-weighted orbit length $\int S\,dl / \int S\,dV$ vs the breadth of the source distribution for an array of proton detectors oriented as in (a); $j \propto [1 - (r/a)^2]^4$. Half the reactions in an emission profile of the form $rS(r) \propto r[1 - (r/a)^2]^i$ occur within the source width r/a.

to detectors that measure protons produced away from the magnetic axis increases as the emission profile broadens.

For measurements of the emission profile, the orientation and position of detectors near the vacuum vessel wall are selected to minimize the sensitivity of the flux to the tokamak poloidal field. For measurements of the poloidal field, on the other hand, it is desirable to orient the detector so that the portion of the plasma it views depends sensitively on the poloidal field. This condition is satisfied by orientations viewing any circulating particle, but the configurations most sensitive to poloidal field view orbits for which the vertical drift motion [Eq. (2)] and the free-streaming motion [Eq. (1)] nearly cancel at the midplane (orbits for which the cancellation is exact are known as "stagnation"[20] or "pinch"[22] orbits). When on stagnation orbits, 3-MeV protons typically have a (counter) parallel velocity of $v_\parallel / v = -0.3$. For these configurations, small changes in the poloidal field dramatically alter the type of orbit viewed (Fig. 3).

Consider one detector that is oriented to measure the emission profile (Fig. 1), and another detector that accepts protons whose orbits are sensitive to the poloidal field (Fig. 3). If the field is relatively strong, the proton orbits measured by the field-sensitive detector originate closer to the magnetic axis than the ones measured by the emission-profile detector, so the flux of protons is larger at the field-sensitive detector. If the field is relatively weak, the proton orbits originate farther from the magnetic axis than the ones measured by the emission-profile detector and the flux of protons is smaller at the field-sensitive detector. The relative flux at the two detectors provides information about the poloidal field distribution.

To make the discussion more concrete, consider a specific design. The emission profile is measured with an array of detectors oriented to view orbits as in Fig. 1. Three detectors are oriented to view near-stagnation orbits as in Fig. 3. The flux at these detectors is a very strong function of the distribution of the plasma current (Fig. 4). To the extent that the flux at the detector is determined primarily by the emissivity of the point of closest approach to the magnetic axis of the viewed orbit, measurement of the flux constitutes a measurement of this point-of-closest approach. The poloidal field is then determined by the requirement that the field moved the proton from the point-of-closest approach to the detector. In general, this requirement does not uniquely determine the magnetic field since the proton is affected by the field all along its trajectory to the detector; however, if the current distribution is smooth and monotonically decreasing, the proton trajectory is most strongly affected by the poloidal field in the region around its near-stagnation point. A sensitivity analysis indicates that, for near-stagnation orbits, the protons are most sensitive to the poloidal field within $\pm$ 5 cm of the part of the orbit where the free-streaming motion [Eq. (1)] nearly cancels the vertical drifts [Eq. (2)]. The physical explanation for this result is that the protons spend more time around a near-stagnation point than in other regions of the plasma so the horizontal displacement of the proton orbit [which is proportional to the poloidal field through Eq. (1)] is most strongly affected by the field in this

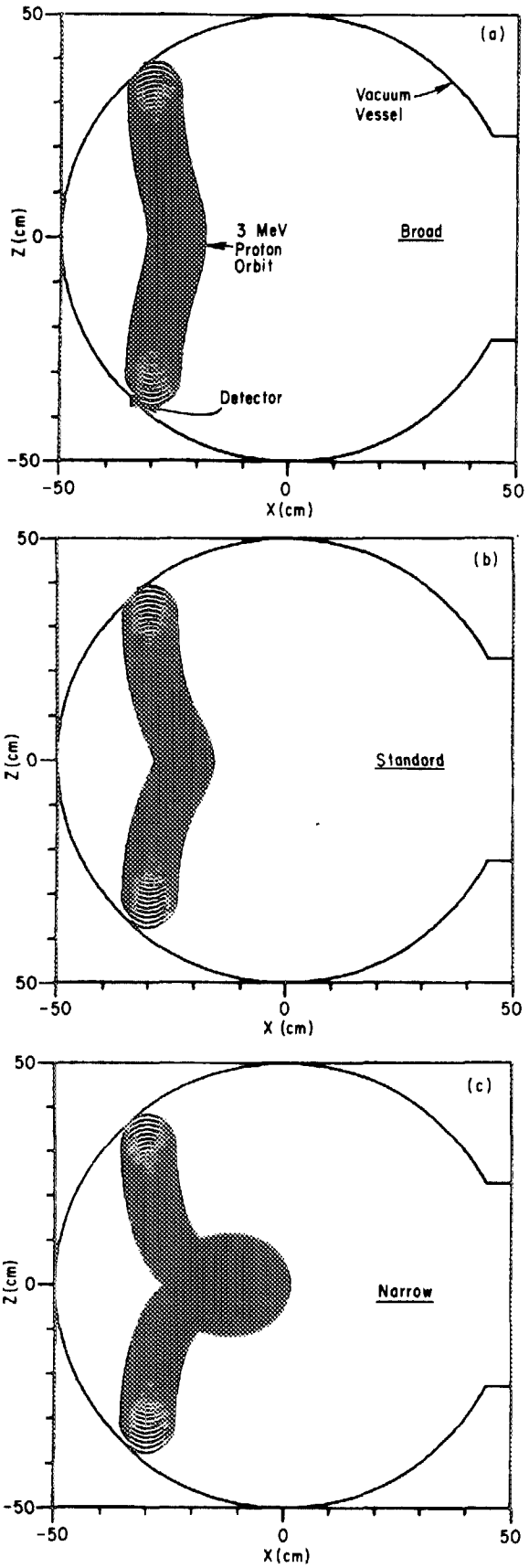

FIG. 3. Poloidal projection of 3-MeV proton orbits in PLT for three different model current profiles. The total plasma current ($I_\phi = 430$ kA) and detector orientation and position ($R = 98$ cm; $z = -36$ cm; $\sin v_\phi/v = 0.06$) are identical in (a)–(c). The model current profile is $j \propto [1 - (r/a^2]^i$, with $i = 2$ (a), $i = 4$ (b), and $i = 6$ (c). $B_\phi = 32$ kG; $a = 40$ cm; $R_0 = 132$ cm.

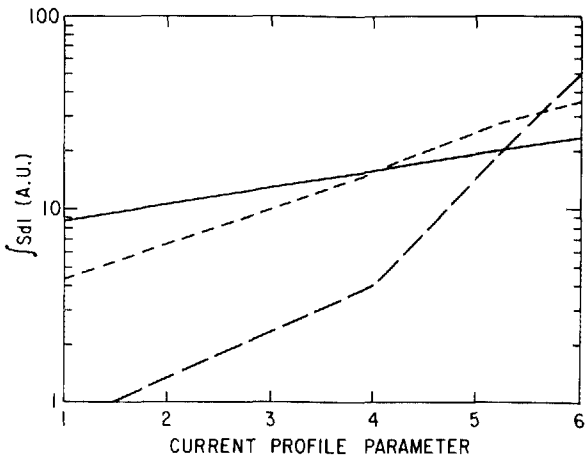

FIG. 4. Emission-weighted orbit length $\int S\,dl$ vs the breadth of the plasma current profile for three detectors. The detectors are assumed to be oriented to measure near-stagnation orbits (Fig. 3) at radial positions of $R = 98$ cm (long dash), $R = 108$ cm (short dash), and $R = 118$ cm (solid). The current is assumed of the form $j \propto [1 - (r/a)^2]^i$, where i is the current profile parameter. A fairly broad thermonuclear profile $\{S(r) \propto [1 - (r/a)^2]^9\}$ was used in the calculation. For an actual detector, the quantity $\int S\,dl$ is proportional to the measured flux. The flux at the detectors is larger for more narrowly peaked profiles (larger values of the current profile parameter) because the free-streaming motion [Eq. (1)] becomes relatively larger for larger poloidal field, causing the measured protons to originate closer to the magnetic axis.

region. Since the poloidal field strength falls to zero near the magnetic axis, this technique is suitable for q measurements only for $r/a \gtrsim 0.2$.

The ability to obtain poloidal field information from proton measurements depends on the degree and accuracy of collimation (Fig. 5) and on the accuracy of the emission-profile measurement. Our present detectors (Sec. II) have 5° pitch-angle collimation and $\gtrsim 10\%$ accuracy in the measurement of the proton flux. With similar detectors, the ab-

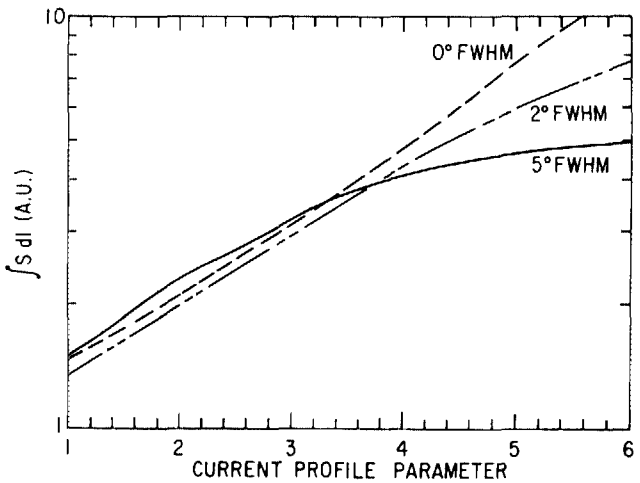

FIG. 5. Average emission-weighted orbit length $\int S\,dl$ vs the breadth of the plasma current profile for a detector oriented to measure near-stagnation orbits at $R = 108$ cm. The average is for a detector with a slotted aperture [Eq. (4)], resulting in pitch-angle collimation of FWHM = 0° (dashed line), 2° (short-short-long dash), and 5° (solid), respectively. The current is assumed of form $j \propto [1 - (r/a)^2]^i$, where i is the current profile parameter. $rS(r) \propto r[1 - (r/a)^2]^9$. For an actual detector, the quantity $\int S\,dl$ is proportional to the measured flux. The greater sensitivity of the curve with ideal collimation (0°) to the current profile parameter than the curves with finite collimation indicates that more accurate measurements of the field are possible with a narrowly collimated detector.

solute accuracy of poloidal field measurements achievable at $r/a = 0.5$ is $\pm 25\%$.

The techniques described above rely on comparison of the proton flux at different pitch angles. Implicit in the discussion is the assumption that the proton emission is isotropic in pitch angle. This is certainly true for the prompt losses of 3-MeV protons from a thermonuclear plasma; however, initially confined orbits that subsequently escape the plasma probably do not populate all unconfined orbits uniformly. Although these "nonprompt" unconfined protons could conceivably cause the result of an experiment to be misinterpreted, it seems unlikely that they were an appreciable source of error in our experiments. Protons that escape after they have lost an appreciable fraction of their energy ($\gtrsim 20\%$) do not pose a problem regardless of loss mechanism since these protons can be rejected using energy spectroscopy. Protons that escape by pitch-angle scattering into the loss region are expected to accumulate preferentially near the loss boundary. As long as protons only scatter anomalously rapidly, but do not scatter anomalously large angles, one can avoid anisotropies introduced by this mechanism by viewing orbits that are not too near the loss boundary. A redistribution of ions spatially can also generate anisotropies in the loss region of velocity space by moving protons into a region where the loss boundary is shifted. In other words, barely confined ions that drift from their birth position to another position are likely to strike the walls, but the flux of these ions at any given point on the vessel is not expected to be uniform in velocity space. Unless the drift is rapid, however, a formerly confined proton's trajectory will intersect the limiter before the proton can drift out far enough to strike a detector mounted on the vessel wall. Thus, a particle must drift ~ 10 cm in a drift orbit period ($\sim 1\ \mu$s) in order to contribute to the flux incident on a detector. Transport this rapid may occur during sawtooth events[23,24] or "fishbone" instabilities.[25] As with anomalous pitch-angle scattering, velocity-space anisotropy created by rapid spatial drifts is likely to occur (if it occurs at all) primarily near the loss boundaries in phase space. Viewing orbits that are not too near loss boundaries therefore reduces the likelihood that either mechanism will significantly affect the flux measurements. Usually, orbits selected for emission-profile measurements are not close to loss boundaries. For example, the orbits in Fig. 1 are about 20° from the loss boundary. On the other hand, stagnation orbits usually lie on the loss boundary so the near-stagnation orbits of Fig. 4 are 3°, 8°, and 12° from the loss boundary, respectively, for "normal" current profiles ($i = 4$). Of the detectors used in our experiments (Sec. II), the detector that views protons closest to a loss boundary views protons 9° from the boundary. The flux of low-energy protons measured by this detector is not correlated with the magnitude of the plasma current (changing the current moves the proximity of the boundaries in velocity space; see Sec. II F), so scattering across the loss boundary probably was negligible in our experiments.

Calculations of the effect of stray fields on the proton orbits indicate that a 100-G stray field only changes the detection efficiency by a few percent. Toroidal field ripple, electric fields of O(1keV), Doppler broadening of the proton energy, and 2% errors in the measurement of the plasma current I_ϕ also result in small changes in the predicted flux.

II. COLLIMATED PROTON DETECTORS

In Sec. I, proton emission profile and poloidal field diagnostics were described in terms of single-proton orbits (Figs. 1 and 3). Of course real proton detectors do not measure protons created on a single orbit. The detectors actually measure a quantity called the absolute detection efficiency ϵ (defined as the ratio of the number of counts detected to the total number of particles emitted), which does depend on the properties of individual proton orbits, but which also depends on the size of the detector and the degree of collimation. Usually, the total number of particles emitted is determined by simultaneous measurement of the magnitude of the 2.5-MeV neutron emission from the $d(d,n)^3$He fusion reaction, which, for reactant energies less than about 60 keV, is virtually identical to the magnitude of the $d(d,p)t$ emission. In an actual experiment, the detection efficiencies of different detectors are compared to deduce the emission profile and the poloidal field.

In this section, a formula for proton detection efficiency is presented[26] (Sec. II A) and the detectors used in our PLT experiments are described (Sec. II B). Next, the design criteria for narrowly collimated detectors (Sec. II C) and the collimation properties of our PLT detectors (Sec. II D) are described. Then, the accuracy of our measurements of the proton flux is discussed (Sec. II E). The section concludes with a discussion of the effect of scattering from collimator walls on measurements of the proton detection efficiency (Sec. II F).

A. Formulas for detection efficiency

The properties of MeV ions permit several approximations that allow accurate calculation of the absolute efficiency ϵ of a proton detector configuration. The intrinsic efficiency of the surface barrier detectors used to measure the protons is virtually unity. The MeV ions that strike solid surfaces lose energy about 1000 times faster than they scatter, so metal apertures can be considered perfect openings with "black" walls and all protons that strike the detector can be assumed to originate in the plasma (Sec. II F). The classical slowing-down time for unconfined fusion products born in the plasma is 10^3–10^4 times longer than the transit time to the wall so MeV ions escape the plasma on trajectories governed by the Lorentz force law, with negligible probability of colliding with plasma particles. Since the proton equations of motion are Hamiltonian, phase space is conserved by the mapping that relates ions born in the plasma to the phase space subtended by the detector.[27] In other words, the six-dimensional volume formed by the detector and its collimating apertures is equal to the six-dimensional volume of the plasma that emits the protons measured by the detector. Calculation of these volumes[21] yields the formula for detection efficiency ϵ,

$$\epsilon = \frac{A \int d\Omega\ T(\Omega) \int S\, dl}{4\pi \int S\, dV}, \tag{3}$$

where A is the surface area of the detector, $S(\mathbf{r})$ is the fusion emissivity, dl is the differential length of the proton orbit, and dV is the plasma volume element. The transparency $T(\Omega) \leqslant 1$ is the fraction of the detector that measures protons incident with angle Ω. While $\int S\, dl$ depends on the position of the detector with respect to the plasma source and on the orbits of protons from the plasma to the detector, the quantity $AT(\Omega)$ depends only on the geometry of the detector-aperture system.

Consider protons incident at angle θ on the idealized, one-dimensional, detector-aperture configuration sketched in Fig. 6(a). Some protons enter the entrance slit of length $2x_a$ and travel on straight orbits to the detector of length $2x_a$, which is separated from the entrance slit by a length d. Other protons strike the walls of the slit or miss the detector and are lost. A proton travels a distance $x_p = d \tan\theta$ in the x direction between the entrance slit and the detector. By construction, the length L_x of the detector irradiated by protons incident at angle θ is

$$L_x T_x(\theta) = \begin{cases} 2x_{\min} \cos\theta & |d\tan\theta| < |x_d - x_a| \\ (x_a + x_d - |d\tan\theta|)\cos\theta & |x_d - x_a| \leqslant |d\tan\theta| \leqslant x_a + x_d \\ 0 & x_a + x_d < |d\tan\theta|, \end{cases} \tag{4}$$

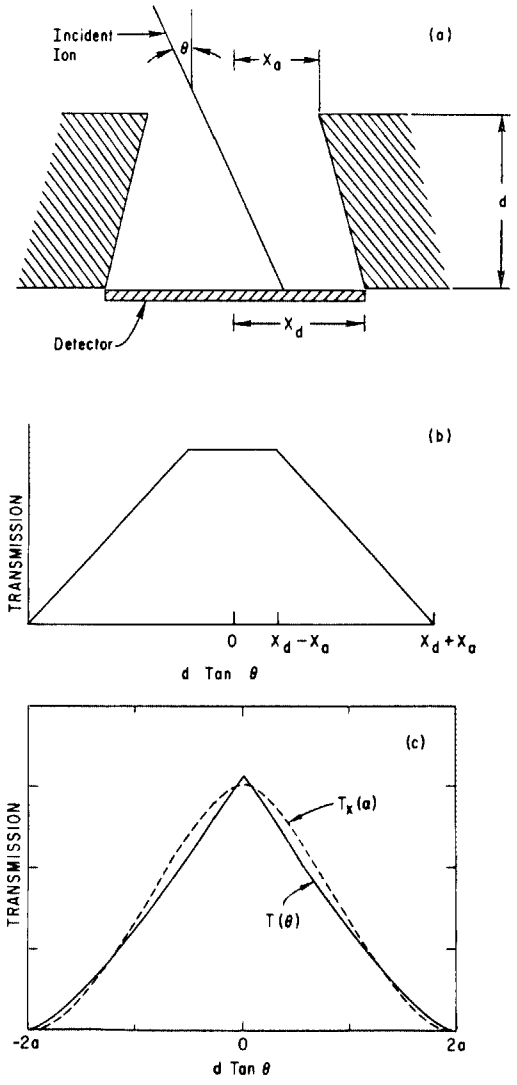

FIG. 6. (a) Incident ions pass through a slotted aperture $2x_a$ wide and d deep and strike a detector $2x_d$ wide. (b) Transmission for a slotted aperture as a function of incident angle θ [Eq. (4)]. (c) Transmission $T(\theta)$ for a circular aperture of radius a and depth d as a function of incident angle θ. $T_x(a)$ is the one-dimensional transmission function for circular holes [it is analogous to the transmission function for one-dimensional slots, Eq. (4)], $T_x(\alpha) = \int d\beta T(\theta;\alpha,\beta)$, where $\tan^2\theta = \tan^2\alpha + \tan^2\beta$.

where $x_{\min}$ is the smaller of x_a and x_d. For a deep slot ($\theta \ll 1$) and $x_a \simeq x_d$, the transmission of a slotted collimating aperture approximates a triangle function [Fig. 6(b)] with FWHM $= (x_a + x_d)/d$. The transmission of a two-dimensional slotted collimator is the product of two terms of the form of the one-dimensional transmission function [Eq. (4)].

Another configuration of interest is a circular hole of radius a and length d with a detector at one end. In this case the area of the detector illuminated by a beam of protons incident at angle θ is given by the intersection of two circles with centers displaced a distance $d\tan\theta$. Calculation of this area yields

$$AT(\theta) = \begin{cases} 2a^2 \cos\theta \left[\pi/2 - |x|\sqrt{1-x^2} - \sin^{-1}(|x|)\right], \\ \quad |x| \leqslant 1, \\ 0, \quad \text{otherwise}, \end{cases} \tag{5}$$

where $x \equiv (d\tan\theta)/2a$. The FWHM of a deep circular collimator differs by less than 5% from the FWHM of a slotted collimator of equal area and depth [Fig. 6(c)].

So far in our treatment of collimating apertures we have assumed straight proton orbits. Actual proton orbits in a magnetic field are helical rather than straight, however. Intuitively, if the gyroradius of the proton orbit ρ is much larger than the depth of the collimator d, the approximation of straight proton orbits will be a good one and the expressions, Eqs. (4) and (5), are valid. On the other hand, for $\rho \lesssim d$, some protons predicted by Eqs. (4) and (5) to strike the detector will curve off and strike the walls of the aperture structure before reaching the detector. Analysis of such "vignetting" indicates that the transmission of the hole depends primarily on a single geometrical factor.[21] For

$$\rho \gtrsim 5d^2/16a, \tag{6}$$

little vignetting occurs and the "straight orbit approximation" is a good one. In practice, the criterion expresed in Eq. (6) is satisfied rather easily. For the collimators used in our experiments (Sec. II B), the effect of proton curvature on the efficiency of the detectors is negligible.

The numerical evaluation of Eq. (3) is described in the Appendix.

B. PLT detectors

Seven collimated 3-MeV proton detectors (Fig. 7) were installed in PLT for emission profile and poloidal field mea-

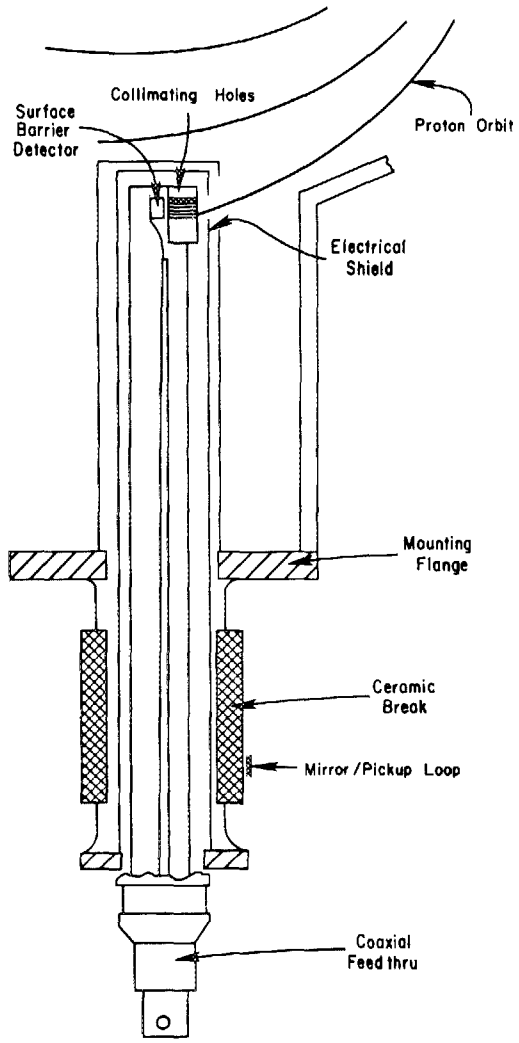

FIG. 7. Schematic diagram of a 3-MeV proton detector installed on PLT. The protons pass through the electrical shield at an opening covered by 90% transparent screen of 0.003-in.-diameter stainless-steel wires. The collimating holes consist of ~150 holes (0.0135-in.-diameter by 0.150 in. deep) drilled at an angle in a stainless-steel block. The protons are measured by a ruggedized ORTEC silicon surface barrier detector. The detector has a rectangular active area (2.5×0.3 cm) and a depletion depth of about 130 μm. A 13-μm beryllium foil protects the front surface of the detector. The detector assembly is mounted onto a port in the tokamak using the gold-seal mounting flange.

surements. It was originally intended that four of the detectors be oriented to measure the emission profile and that three of the detectors be oriented to measure the poloidal field. In order to collimate the incident protons, about 150 small (0.0135-in. diameter) holes were drilled at an angle in a 0.75-cm^2 region of a block of stainless steel 0.15-in. thick. The angle of the holes for each of these "collimators" was selected so that each detector assembly (Fig. 7) would measure protons with the desired incident velocity with respect to the magnetic field. The collimators were fastened to a box called the "detector holder" that positioned a surface barrier detector directly beneath the collimating holes. Provision was made to measure accurately the actual orientation of the proton collimators upon installation in the tokamak, but a capability to adjust the orientation of the detectors after installation was not included in the design. During an opening of the tokamak to atmosphere, the assembled and tested detectors were rigidly mounted on vacuum ports. After the tokamak resumed operation, measurements of the orientation of the proton collimators (Sec. II D) indicated that the installed detectors typically deviated 5–10° from the intended orientations, primarily due to mechanical uncertainties in the PLT vessel. In future experiments, a significant improvement could be made by permitting alignment of the detector assembly *in situ*.

Even though the proton detectors were not oriented as originally intended, the data from the detectors still contain information about the emission profile and the poloidal field (Sec. III). Orbits viewed by the assembled detectors are plotted in Fig. 8. One of the detectors (P118) views an orbit that is quite sensitive to the plasma current (Fig. 19). Five of the detectors view orbits that are fairly insensitive to changes in the poloidal field. Data from these detectors are used to deduce the $d(d, p)t$ emission profile (Fig. 17). Most of the proton orbits incident on the seventh detector (P150A) are obstructed by an adjacent wall (Sec. II C) so the data from this detector are not useful for measurements of the emissivity or of the poloidal field. The properties of the assembled array detectors are summarized in Table I.

C. Design criteria for proton collimators

In this subsection, design criteria for experiments with accurately collimated proton detectors are presented. The objective of these proton experiments is to deduce the emission profile S and the poloidal field B_θ from the relative

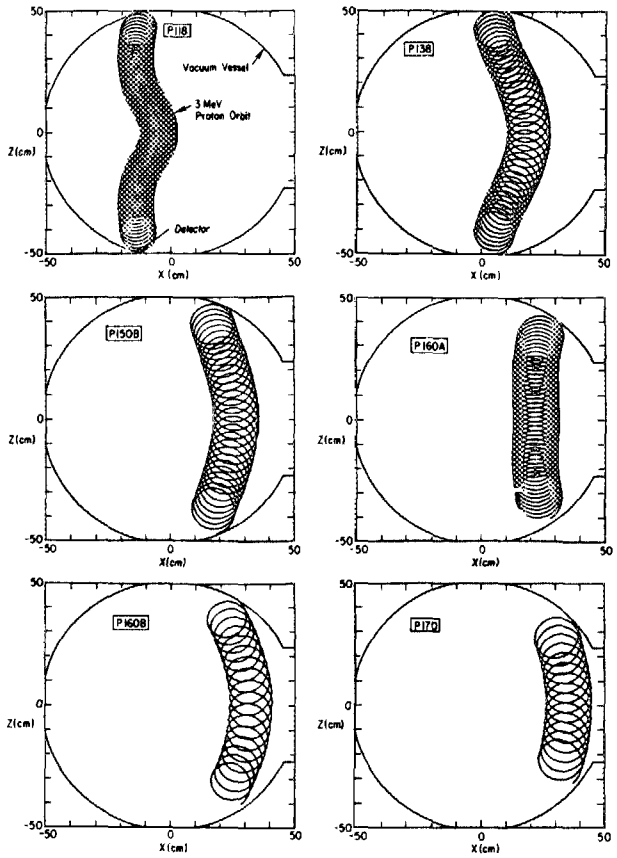

FIG. 8. Poloidal projection of the orbits measured by the 3-MeV proton array for $I_\phi = 400$ kA, $B_\phi = 31$ kG, $j \propto [1 - (r/a)^2]^4$.

TABLE I. Collimation properties of the PLT 3-MeV proton array.

Name of assembly	Major[a] radius (cm)	Vertical[b] position (deg)	Gyroangle[c] (deg)	Collimator[d] angle (deg)	Mirror[e] angle (deg)	Pitch[f] angle (deg)	Collimator[g] FWHM (deg)	Transparency[h]
P118	118.4	−49.2	0.6	12.8	−4.0	8.8	4.9	0.91
P138	137.9	−49.8	10.3	0.3	−4.4	−4.1	4.9	1.0
P150A	150.2	−47.0	10.3	0.6	1.1	1.7	4.8	1.04
P150A	150.2	−47.0	10.9	−1.0	−6.6	−7.6	5.4	1.34
P160A	159.8	−40.5	−4.0	−4.3	13.8[i]	9.5	4.7	0.98
P160B	159.8	−40.5	−1.7	−12.5	−11.4[i]	−23.9	4.8	1.16
P170	169.3	−31.9	−10.9	−14.5	−4.3	−18.8	4.6	0.22

[a] The major radius of the vacuum vessel is 131.8 cm.
[b] With respect to the midplane.
[c] With respect to the normal to the flange; + means the orbit points up from the detector.
[d] Angle between maximum of transparency and normal to alignment mirror.
[e] Angle between alignment mirror and major radial direction.
[f] Angle between horizontal component of incident proton velocity and major radial direction; + indicates co-going protons.
[g] With gyroangle adjusted to maximize transparency.
[h] $\int T(\Omega)d\Omega$ divided by transparency of P138.
[i] The bolt circle of these assemblies is rotated ± 15° from the radial direction.

count rates of several detectors using Eq. (3). Quantitative conclusions concerning S and B_θ require accurate determination of the quantity $AT(\Omega)d\Omega$ (the effective area AT of a detector for protons incident at angle Ω) for the various detectors. An important design criterion for proton experiments is, therefore, that the collimation and transparency of the detector assemblies can be accurately calibrated in the absence of the tokamak magnetic fields. This implies that all protons traveling on orbits that pass through the collimating holes must do so without encountering obstructions. Consider the orbit of a 3-MeV proton near the vacuum vessel wall [Fig. 9(a)]. Protons traveling on orbits that lead to the detector can be obstructed either by the top edge of the detector assembly or by the vessel wall itself. In general, the fraction of orbits that *would have* traveled into the opening of the detector if there were no obstructions is a complicated function of the toroidal field, of the poloidal field, and of the detector-wall geometry. Measurement of this quantity would require an *in situ* experiment with a known source of 3-MeV protons and the full tokamak magnetic fields. These considerations dictate that the collimating holes accept only a narrow range of gyroangles and that the distance between the detector and the top of the detector assembly be $\lesssim 1.2$ cm.

One indication that the proton orbits are free from obstructions is to measure the toroidal field sensitivity of the detectors. If the orbits are unobstructed, the proton flux is expected to vary only weakly with toroidal field, since the main effect of toroidal field on the path of a proton is to increase its gyroradius. For a partially obstructed detector, however, the flux is expected to depend strongly on field since small changes in field can completely vignette the detector [Fig. 9(b)]. Data from a toroidal field scan with our 3-MeV proton array appear in Fig. 10.

The strong toroidal field dependence of P150A (Fig. 10) suggests that protons incident on this detector may be obstructed by an adjacent wall. At first glance, this hypothesis

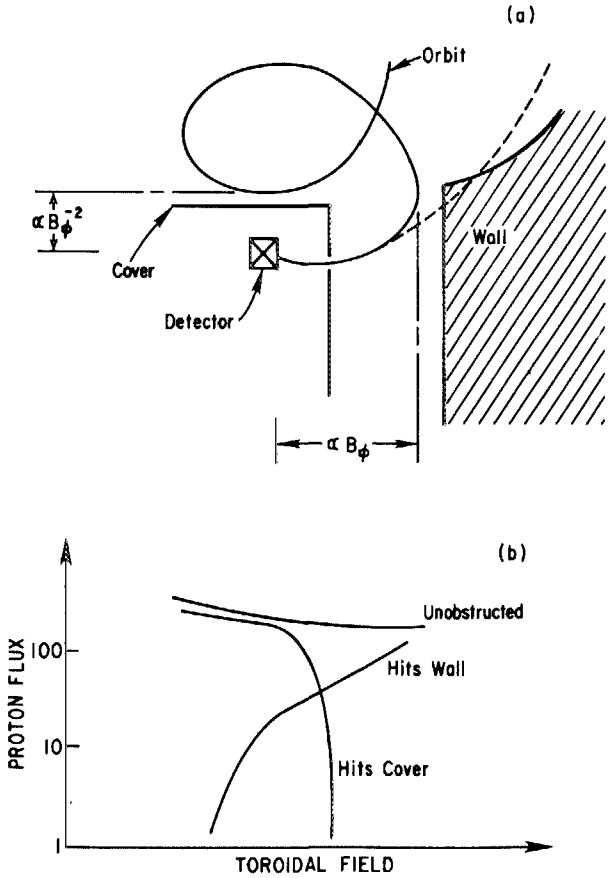

FIG. 9. (a) Sketch of a proton orbit (not to scale) near the entrance of the detector. Protons can be obstructed by neighboring walls if the proton gyroradius (7 cm at 32 kG) is too large (dotted orbit) or by the protective cover of the detector assembly if the downward drift motion between successive gyroloops is too small. The distance between successive gyroloops for perpendicular ions is approximately $(2\pi E)/(m\Omega^2 R) = 1.4$ cm for 3-MeV protons at 32 kG, where E is the ion energy, m the ion mass, Ω the ion cyclotron frequency, and R the major radius of the detector. (b) If the proton orbits incident on the detector are partially obstructed, the measured proton flux is expected to depend strongly on the toroidal field. The curves are sketches of the expected dependencies.

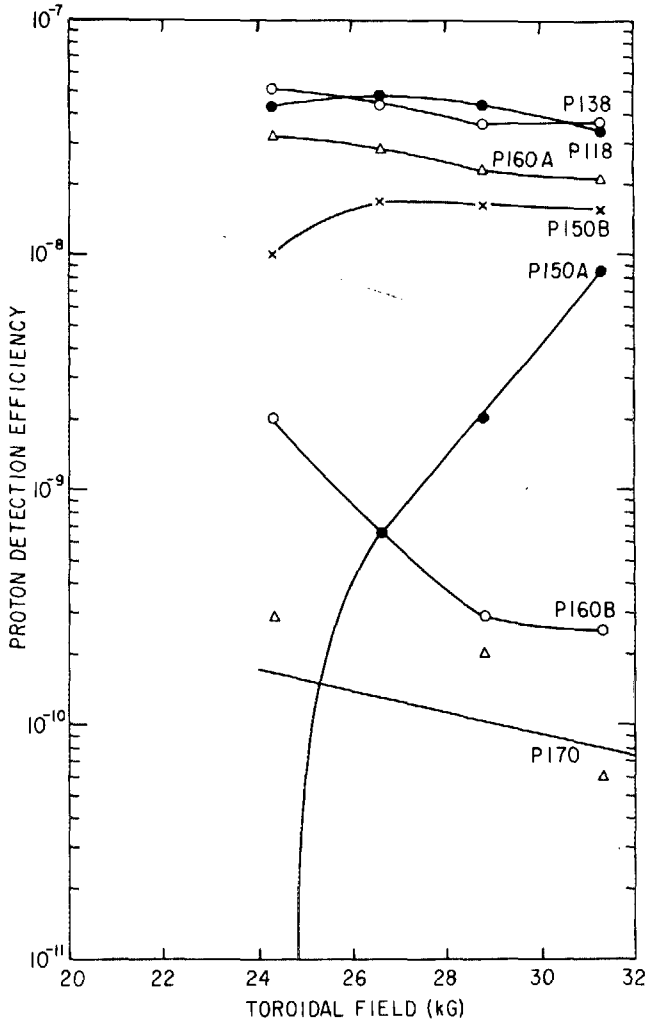

FIG. 10. Proton detection efficiency [proton counts divided by $d(d,n)$ emission] vs toroidal field for the 3-MeV proton array during steady-state ohmic heating ($I_\phi = 430$–470 kA; $\bar{n}_e = 2.5\times10^{13}$ cm^{-3}; deuterium fill gas) in PLT. For $\epsilon \gtrsim 10^{-8}$, the relative accuracy of the measurement was typically $< \pm 1\%$; for $\epsilon \sim 3\times10^{-10}$, the typical error due to counting statistics was $\pm 50\%$.

appears inconsistent with the results of the measurement for P150B, which was mounted in a port nominally identical to the one occupied by P150A but at a different toroidal location. The data for P150B indicate a weak toroidal field dependence for $B_\phi \gtrsim 26$ kG with some appreciable vignetting possibly occurring for $B_\phi \lesssim 24$ kG. A careful analysis of the expected toroidal field dependence of the two detectors due to vignetting, however, indicates that a good fit to the measured data can be obtained by assuming that the wall beside P150A is 3 mm higher with respect to the detector than the wall beside P150B.[21] A 3-mm distortion of the relative position of the PLT wall with respect to the detector appears consistent with the tolerances and distortions of the PLT vacuum vessel and of the detector height. This fit to the 3-MeV proton data implies that, at $B_\phi \simeq 28$ kG, the detection efficiency of P150A was reduced an order of magnitude due to protons intersecting the vacuum vessel wall prior to reaching the detector, but that the reduction in detection efficiency of P150B was negligible.[21] Figure 10 also indicates that the detection efficiency of P160B depends on toroidal field. This dependence is too weak to be due to proton orbits that strike the cap of the detector before looping into the detector [Fig. 9(a)], however. The probable explanation for the toroidal field dependence of P160B is that as the toroidal field is reduced, the gyroradius of the 3-MeV proton increases, allowing the detected proton orbits to sample a region of higher emissivity.

To act as a collimator, the collimating structure must contain walls that prevent tunneling between adjacent openings. Protons that do cross walls must lose sufficient energy to be rejected using energy discrimination. This implies that stainless-steel barriers must be $\gtrsim 0.001$ in. thick and that aluminum barriers must exceed 0.002 in. Furthermore, barriers should be free from imperfections so that protons that bore through ragged edges (Sec. II F) do not degrade the energy resolution of the measurements. The collimating holes for our 3-MeV proton array are separated from one another by about 0.012 in. of stainless steel.

A perfectly collimated detector of infinitesimal size measures protons born on a single orbit (a line in phase space). Real detection systems do not measure a line in phase space but accept a range of proton drift orbits. If we label the proton orbit by its guiding center position θ and its pitch angle χ ($\cos\chi \equiv v_\parallel/v$) at the detector, then the more narrow the range of χ and θ for these measurements, the better defined the spatial region in the plasma from which the emission emanates. The range in θ of the measurement is determined by both the poloidal extent of the detector and by the collimation in gyroangle. To reduce the poloidal extent of the detector, the detector is oriented with its length in the toroidal direction and its width (0.3 cm) in the minor radial direction. A range in gyroangle $\Delta\varphi$ only results in a displacement in poloidal angle of $\Delta\theta \simeq (\rho/a)\Delta\varphi \simeq 0.18\Delta\varphi$ so the measurement does not require particularly narrow collimation in gyrophase to achieve good definition of the guiding center position. In practice, the angular acceptance in the poloidal plane is determined by the requirement that accepted orbits be free from obstructions [Fig. 9(a)].

Since they view orbits that have little free-streaming motion anyway, the sensitivity to the degree of pitch-angle collimation is not very strong for detectors oriented to measure the emission profile (Fig. 11). This is in contrast to detectors oriented to measure the poloidal field, which are extremely sensitive to the degree of pitch-angle collimation (Fig. 5).

Narrow collimation reduces the flux of particles incident on the detector, thereby degrading the time resolution of the measurement. The ideal collimator for these diagnostics consists, therefore, of many narrow openings separated by ~ 0.001 in. of material. The actual collimators fabricated for the 3-MeV proton array consist of ~ 150 small holes (0.013-in. diameter by 0.150-in. thick) drilled in a 0.75-cm^2 region of a block of stainless steel. These collimators have a FWHM of $\sim 5°$ and a maximum transparency of $\sim 15\%$. With these collimators, the detection efficiency for centrally viewing detectors is typically 10^{-8}, which implies a time resolution of ~ 0.5 s during ohmic heating in PLT and of ~ 5 ms in PLT deuterium beam-heated discharges.

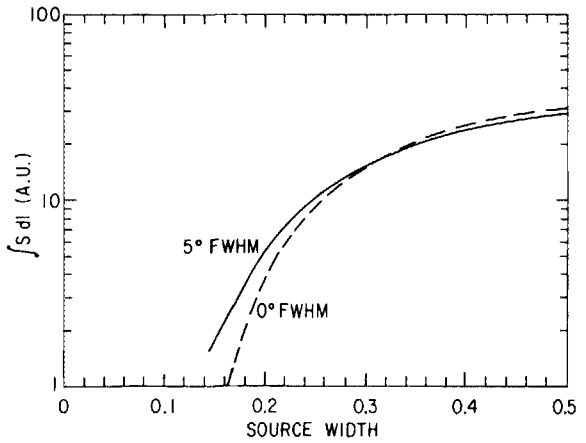

FIG. 11. Normalized emission-weighted orbit length $\int S\,dl / \int S\,dV$ vs the breadth of the source distribution of an emission-profile detector at $R = 118$ cm. Half the reactions in an emission profile of the form $rS(r) \propto r[1 - (r/a)^2]^i$ occur within the source width (r/a) plotted on the abscissa. The average is for a detector with a slotted aperture [Eq. (4)], resulting in pitch-angle collimation of FWHM = 0° (dashed line) and 5° (solid), respectively. The peak of the transparency was $\sin v_\phi/v = 0.35$ (dash) and $\sin v_\phi/v = 0.38$ (solid); $j \propto [1 - (r/a)^2]^4$. For an actual detector, the quantity $\int S\,dl$ is proportional to the measured flux. For a detector that views protons born away from the magnetic axis, the flux is larger for broader emissivity profiles. The similarity between the curve with finite collimation (5°) and the curve with ideal collimation (0°) indicates that accurate measurements of the emissivity profile are possible with detectors with finite collimation.

D. Measurements of detector collimation

This subsection describes a calibration experiment that measured the collimation and transparency of each of the detectors in the PLT 3-MeV proton array. The calibration was accomplished in two stages. First, the transmission was measured as a function of detector orientation Ω with respect to a reference orientation Ω_0 before the detector was installed in the tokamak and, second, the reference orientation Ω_0 was related to the toroidal field after the detector assembly was mounted onto PLT.

In the first stage of the calibration, the effective area of the detectors was measured as a function of angle using ~5-MeV alphas from a radioactive source to simulate protons. The apparatus for the measurements consisted of a HeNe alignment laser and associated beam-steering optics, a rough vacuum chamber and radioactive isotope, and a two-stage rotation stand (Fig. 12). The experimental procedure was as follows: A pickup loop and a plane mirror mounted on an acrylic spool were epoxied to each of the detector assemblies on the ceramic break beneath the vacuum seal flange (Fig. 7). The detector assembly was mounted in the two-stage rotation stand. The orientation of the detector was then adjusted until the HeNe laser beam passed through a pinhole about 40 in. from the rotation stand, reflected off the mirror mounted on the detector assembly, and returned through the pinhole, indicating that the mirror was perpendicular to the incident beam. The accuracy of the alignment, which was limited by laser divergence and by the finite sizes of the mirror and pinhole, was better than 0.2°, which was the backlash of the rotation stand. A 5-mCi, ^{244}Cm radioactive source was then mounted directly behind the pinhole. After the chamber was evacuated, the orientation of the detector assembly was rotated and the fluence of alphas was measured as a function of

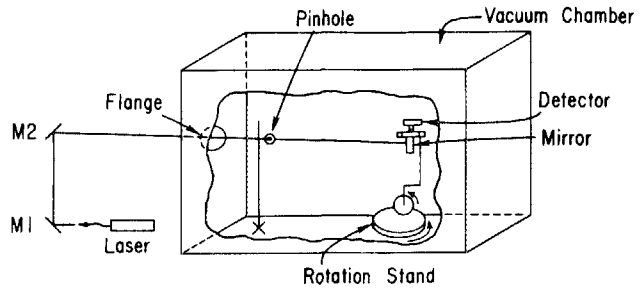

FIG. 12. Sketch of the apparatus used to measure the collimation of the 3-MeV proton detectors used for emission profile and poloidal field measurements. After aligning the detector assembly with the laser, a radioactive alpha source was mounted on the pinhole and the fluence at the detector as a function of angle of rotation was measured. The distance from the alpha source to the detector was typically 40 in.

rotation angle. To reduce the error associated with counting statistics below other errors introduced by the calibration procedure, the sampling time was adjusted so that at least 2000 counts were collected near the maximum of the transparency, which is equivalent to an error of $\pm$ 3% in the measurement of the FWHM of the transparency function.

This procedure resulted in a matrix of measurements of the fluence as a function of a pair of angles of rotation that were measured relative to a particular zero angle (the normal of the laser alignment mirror). In order to normalize the fluence measurements of the collimated detector assemblies, a measurement was made of the fluence incident on an entirely uncollimated detector oriented normal to the source [for which $T(\Omega) = 1$]. The agreement between the results of these measurements (Fig. 13) and theoretical predictions for the transparency $T(\Omega)$ is good (Fig. 14). The only significant discrepancy is that the fit to the data appears to be improved if the collimating holes are assumed to be 4% larger than the 0.0135-in. diameter bit used to drill the holes. Due to tool chatter, the holes may be wider than the bit. Alphas that reach the detector after undergoing a grazing-incidence reflection from the side of a collimating hole also may contribute to the observed broadening. Estimating the effective angular broadening $\Delta\psi$ of the holes due to channeling using Lindhard's formula[28] gives $\Delta\psi \simeq 0.5°$. Boring through the

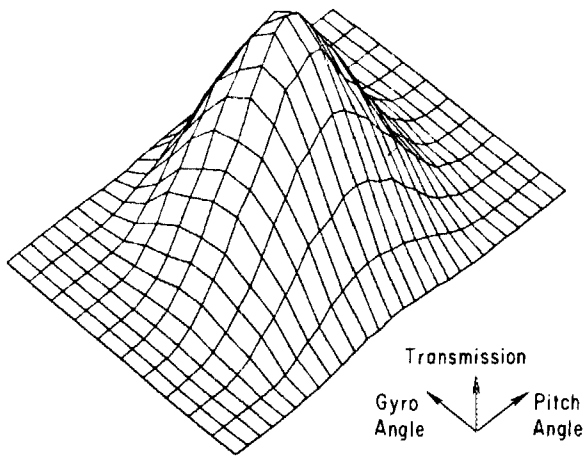

FIG. 13. Alpha fluence as a function of angle of rotation for one of the proton detectors. The data for the other detectors were similar.

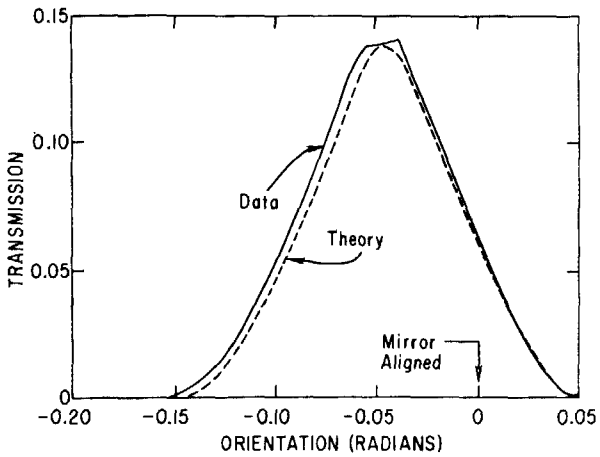

FIG. 14. Alpha transmission as a function of pitch angle with the gyroangle selected to maximize the flux. The dashed curve is the transmission predicted by Eq. (5) (with a small correction for the divergence of the source) for collimator holes that are 0.014 in. in diameter. The angular position of the maximum of the theoretical curve is a fit to the data.

corners of the collimating holes (Sec. II F) also tends to make the holes effectively wider, but estimates of this effect indicate that it is too small to account for the observed increase.

The second stage of the calibration was to relate the reference orientation Ω_0 to the PLT toroidal field. This was accomplished by winding an ~ 12-turn magnetic loop on an acrylic spool that also contained the mirror used to orient the detector assembly with the laser.[21] The deviation of the normal to the magnetic loop from the normal to the mirror is estimated to be no more than $\pm 1°$ due to manufacturing imperfections. The spool was epoxied to the detector assembly with its normal oriented to be nearly perpendicular to the toroidal field once the assembly was installed in PLT. A second, nominally identical, loop also was epoxied onto the ceramic break of the detector assembly with its normal oriented to be nearly parallel to the toroidal field. The relative sensitivity of the two loops and their associated cables and differential amplifiers (Preston 8300 XWB) was measured by placing the detector assembly in a stand in a solenoid and rotating the detector until the signal from the pickup loop was maximized. After the detectors were installed on PLT, the orientation of the detector assembly with respect to the toroidal field was determined by measuring the ratio of the signals in the two coils when the toroidal field was pulsed. The angle of rotation χ_{rot} is

$$\chi_{rot} = \tan^{-1}(kV_{\perp}/V_{\parallel}), \tag{7}$$

where $V_{\perp}$ and $V_{\parallel}$ are the voltages measured by the near-perpendicular and near-parallel pickup loops, respectively, and k is the relative sensitivity of the loops measured in the solenoid. Because dB/dt from the ohmic heating coils is much larger for the perpendicular loop than the change in toroidal flux, the orientation of the detector assembly was not measured during actual plasma shots. The accuracy of the measurement of the angle of rotation with respect to the toroidal field was typically $\pm 0.5°$.

Stray field components produced by toroidal field ripple and by the leads to the toroidal field coils have a less than 0.5° effect on the measurement of the orientation of the collimator.[21]

Unfortunately, because of the small diameter of some of the vacuum seal flanges of the PLT tokamak, it was necessary to complete the assembly of some of the detector assemblies from inside the vacuum vessel after the vacuum seal flange had been mounted. An additional source of error in the case of these detectors is the possibility that the orientation of the collimator with respect to the normal of the alignment mirror may differ from one assembly to the next. To estimate the magnitude of this error, each detector was assembled three times and the orientation of the peak of the fluence with respect to the mirror was measured after each assembly.

The estimated error in the measurement of the orientation of the collimator with respect to the toroidal field is tabulated for each of the detector assemblies in Table II. This error is typically $\pm 1°$, which is adequate for emission-profile measurements. An error of $\pm 1°$ also has a small effect on the overall accuracy of poloidal field measurements made with collimators with an angular spread of 5° FWHM, such as were used in our experiments. The error in the measurement of the transparency of the detector was less than 5%, which is small compared to other errors in the measurement of the proton flux (Sec. II E).

E. Proton flux measurement

For accurate flux measurements, pulse-counting electronics (ORTEC 142 preamplifier, ORTEC 460 amplifier, scalers) were used with the proton detectors in the PLT 3-MeV proton array. Proton spectra measured during ohmic heating are characterized by a relatively narrow width above the proton peak and a broad tail below the peak (Fig. 15). The HWHM of the high-energy side of the proton peak is comparable to the HWHM of the calibration pulser signal (OR-

TABLE II. Errors in pitch-angle calibration of proton detectors.

Name of assembly	Laser alignment (deg)	Spool imperfection (deg)	B_ϕ loop angle (deg)	Reproducibility of assembly (deg)	Total error (deg)
P118	0.2	0.7	0.2	0.3	± 0.8
P138	0.2	0.7	0.2	0.2	± 0.8
P150A	0.2	0.7	0.2	0.7	± 1.0
P150B	0.2	0.7	0.3	0.3	± 0.8
P160A	0.2	0.7	0.5	n/a	± 0.9
P160B	0.2	0.7	0.2	n/a	± 0.8
P170	0.2	0.7	0.2	n/a	± 0.8

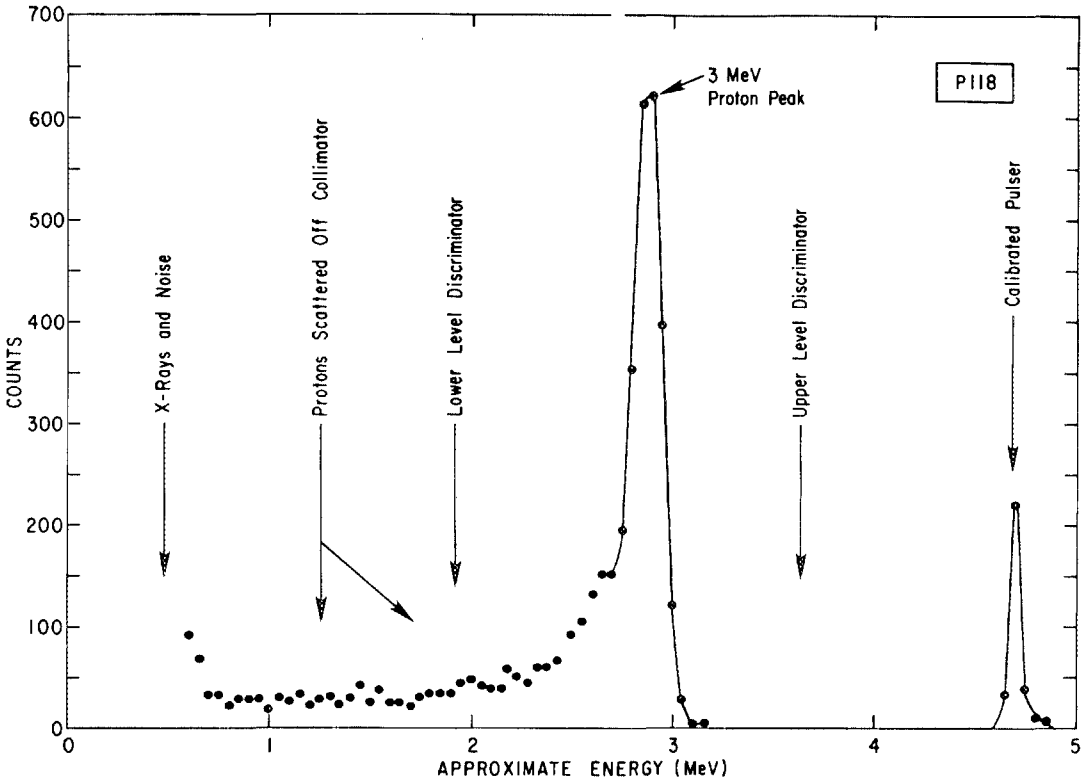

FIG. 15. Energy spectrum measured by P118 during steady-state ohmic heating in deuterium [$I_\phi = 470$ kA; $B_\phi = 31.3$ kG; $\bar{n}_e = 2.5\times10^{13}$ cm^{-3}; $T_e(0) = 1.7$ keV] in PLT ($a = 40$ cm; $R_0 = 132$ cm). Pulses between the indicated discriminator settings are interpreted as protons. The approximate energy scale was determined by replacing the P118 detector assembly with another surface barrier detector that was exposed to a ^{241}Am radioactive source and measuring the 5.3-MeV line produced in the detection electronics.

TEC 480), indicating that the broadening of the proton peak is due to noise in the detection system and is not determined by the energy spread of the incident protons for these thermonuclear plasmas. The broad tail below the peak is thought to be caused by scattering off the collimator (Sec. II F). Counts from x-rays and electronic noise (rising exponentially at low energies) generally make no contribution to the counts in the proton peak.

Energies between the indicated discriminator settings were counted in the flux measurements. Comparison of the spectra from the various detectors in the proton array reveals that the discriminator settings were not positioned identically with respect to the proton peak for all the detectors. This implies that the measured flux must be adjusted when comparing data from different detectors so that the data from each detector reflect the same fraction of the full-energy counts. This adjustment is complicated by an apparent base line shift. When viewed on a pulse-height analyzer, the proton peak appeared to shift as much as 10% (for some of the detectors) when the plasma conditions were changed. The shift was correlated with changes in the dc level of x-ray and noise counts. This shift contributes to the error in the flux measurements since the relationship between the measured number of counts and the actual number of full-energy protons depends on the relative position of the discriminator settings with respect to the proton peak.

For our experiments, uncertainties associated with the setting of the lower level discriminator introduced errors of from 7% (for the detector least sensitive to these errors) to 25% (for the most sensitive detector) in the measurement of the proton flux. The error associated with the positioning of the lower level discriminator is the dominant error in our measurement of the proton flux.

F. Energy loss in collimator walls

In the derivation of the expression for proton detection efficiency [Eq. (3)], it was assumed that the collimating apertures used in the experiments are perfectly "black" or absorbing. Actually, of course, some protons that have collided with the walls of the collimator are detected. Analysis of tokamak 3- and 15-MeV proton spectral measurements[19,29] suggests that most of the low-energy ions observed in the experiments are full-energy ions that have lost energy in the solids surrounding the detectors.

Ideally, the spectral measurements would only reflect the energy distribution of MeV ions in the plasma. For example, it would be desirable to be able to measure initially confined protons that lose some energy in the plasma and then are scattered onto a loss orbit measured by the detector. Such measurements would provide information on the confinement properties of these protons. In the experiments with our 3-MeV proton array, however, the ratio of counts in the low-energy tail to counts in the full-energy peak was observed to be independent of the parameters affecting proton confinement. A tail was observed in the spectrum of all the detectors, despite the fact that some detectors view orbits closer to loss boundaries in velocity space than others. The confinement of 3-MeV protons is predicted to improve at least a factor of 2 between 300 and 450 kA [Fig. 16(a)] but the observed fraction of counts in the low-energy tail did not increase with current (Fig. 16). Spectra for two of the detectors (P118 and P138) accumulated for plasma currents between $I_\phi = 200$–300 kA (most shots $\simeq$250 kA), where virtually no protons are expected to be confined, showed 50% less counts in the tail for one detector (P138) but 75% more counts in the tail for the other detector (P118) relative to 400-KA discharges. The tail was present for $B_\phi = 20$ kG while

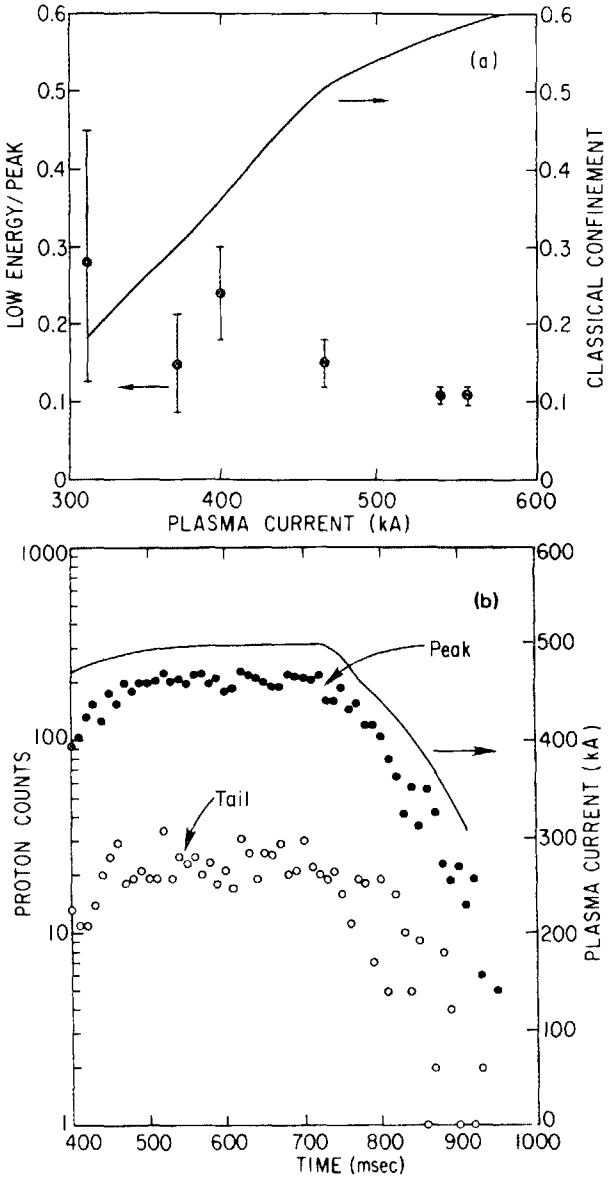

FIG. 16. (a) Ratio of counts between 1.3 and 2.0 MeV to counts in the full-energy peak for P118 as a function of plasma current. Also shown is the average fraction of protons confined in PLT as a function of plasma current.[30] (b) Number of counts in the full-energy peak (in 10-ms bins) and number of counts between 1.3 and 2.0 MeV as a function of time in ohmic discharges with decreasing plasma current. The data are from P118 and are averaged over 29 reproducible discharges.

studies of the burnup of 1-MeV tritons at $B_\phi = 18$ kG on PLT[30] suggest that the 3-MeV proton confinement may have been poor at this low value of toroidal field. In summary, the observed scaling of counts in the tail to counts in the peak indicates that the low-energy protons measured by the 3-MeV proton array detectors did not lose their energy in the plasma.

Another possible explanation for the low-energy counts observed in the experiments is that they are not proton counts but x-ray or electronic noise counts. The counts disappeared when the magnetic field was reversed so this explanation is excluded.

If most of the low-energy counts are due to ions that do not lose energy in the plasma, then the ions must lose energy in the solids surrounding the detector. Protons that strike the walls of the collimator can reach the detector by boring through the edges of the collimator, by pitch-angle (Rutherford) scattering in its walls, or by scattering at grazing incidence (channeling) into the detector. For the collimators used in our experiment, boring through the walls is predicted to be the dominant process and the fractional number of counts f_s that reach the detector with energies between the incident energy E and $E - \Delta E$ is approximately[21]

$$f_s \simeq \frac{4m_e E^2}{\pi d N Z m_i z^2 e^4 \ln B_q}\left(\frac{\Delta E}{E}\right), \tag{8}$$

where d and NZ are the depth and electron density of the collimator, m_i and ze are the mass and charge of the incident ion, and $\ln B_q \simeq 3.5$ for 10-MeV protons in iron. In Table III, the low-energy tail predicted by Eq. (8) is compared with data from three different experiments. The theoretical predictions are consistent with the experimental observations for the 15-MeV proton spectral measurements[29] and for the first 3-MeV proton spectral measurements.[19] The expression, Eq. (8), predicts that the number of counts per bin should be independent of proton energy for protons that bore through the wall, which is also consistent with these experimental observations. For these experiments, most of the measured low-energy protons probably lost their energy boring through the walls of the collimator.

The number of low-energy counts measured by our 3-MeV proton array exceed the prediction of Eq. (8) by a factor of 7 (Table III) and the magnitude of the tail is not independent of energy (Fig. 15). Some of these extra counts are probably protons that lose energy in the 0.003-in.-diameter, stainless-steel, 90% transparent, wire mesh that covers the opening of the detector. The range of a 3-MeV proton in iron is about 0.0022 in.,[31] so about one-third of the protons that strike the wires are expected to have sufficient energy to bore through the mesh, resulting in a predicted increment in the fraction of tail counts of $\lesssim 4\%$ due to this process. It is also possible that the relative number of protons that bore through mechanical imperfections produced by tool chatter is greater for the smaller holes used in our experiments than for the larger holes used previously. Another factor that accounts for at least some of the additional counts measured by the detectors is that the collimators are not uniformly irradiated by protons [as was assumed in the derivation of Eq. (8)] but are frequently more weakly irradiated at angles normal to the collimating holes than at angles that intersect the edges of the collimating holes.

Nonuniform irradiation of the detectors seems to be at least partly responsible for the excess low-energy counts measured by the 3-MeV proton array detectors (Table III). It is experimentally observed that the relative magnitude of the tail is anticorrelated with the magnitude of the flux Γ inci-

TABLE III. Spectral measurements of low-energy protons.

Spectrum	$\Delta E/E$	Tail:peak	Theory[a]	Comments
Ref. 29	3/15	$9\% \pm 2\%$	13%	—
Ref. 19	0.5/3	~1%	0.4%	—
Fig. 15	0.5/3	11%	1.6%	Wire mesh

[a] Equation (8).

dent on the detector. The likely explanation for this effect is that the gradient $d\Gamma/d\Omega$ is largest for detectors that accept protons away from the center of the plasma so that the relative contribution of protons that bore through the walls is larger. This tendency is also apparent in the current dependence of the tail for P118 (Fig. 16): as the current is reduced the detector views a portion of the plasma where the spatial gradient dS/dR is larger, which implies a stronger dependence on pitch angle at the detector. At low current, the tail for P138 is reduced since the detector accepts protons that originate closer to the center of the plasma.

In summary, the low-energy portion of the 15- and 3-MeV proton spectra measured in previous tokamak experiments[19,29] is probably protons that bore through the walls of the collimators. The majority of low-energy counts measured by the 3-MeV array detectors are not protons that lose their energy in the plasma. The low-energy tail measured by these detectors appears to include protons that bore through the collimator walls and protons that bore through the wire mesh that covers the opening to the detector. There is some evidence that the fraction of low-energy counts is enhanced because the flux of protons incident on the detector is not isotropic. With the possible exception of detectors in a strongly nonuniform flux, the assumption of perfectly absorbing walls in the derivation of Eq. (3) (Sec. II A) appears to underestimate the actual proton detection efficiency by less than 5%.

III. SAMPLE PLT DATA

Sample raw data from the PLT detectors least sensitive to poloidal field appear in Fig. 17a. The normalized fluence measurements [detection efficiency ϵ = (proton counts)/(neutron emission)] are plotted versus the radius of closest approach to the plasma center of the proton orbits measured by each detector, yielding a rough emissivity profile. The measurements indicate that, as expected, the fusion emissivity peaks very strongly on axis during ohmic heating. This implies that, although the proton detectors can measure protons created anywhere in a swath a gyrodiameter wide, the dominant contribution to the fluence actually measured by the detectors originated in the few centimeters around the point of closest approach to the magnetic axis of the proton orbits accepted by each detector. It is a good first approximation, therefore, to assume that all protons measured by a detector originated at this point-of-closest approach.

To estimate more accurately the region in which the emission-profile detectors are sensitive, consider the following simplified model. Assume the probability of detection is uniform on a strip a gyrodiameter (2ρ) wide in the X ($X = R - R_0$) direction and infinitely long in the Z direction. Based on the data of Ref. 21, model the emissivity S as an exponentially decaying function of minor radius ($r = \sqrt{X^2 + Z^2}$), $S \propto e^{-r/\lambda}$, where the decay length λ is typically 3–5 cm. Then the detection efficiency ϵ is

$$\epsilon \propto \int_{\text{swath}} S\,dA = 2\int_{X_{\min}}^{\infty} rS(r)\left[\cos^{-1}\left(\frac{X_{\min}}{r}\right) - \cos^{-1}\left(\frac{X_{\min}+2\rho}{r}\right)\right]dr, \tag{9}$$

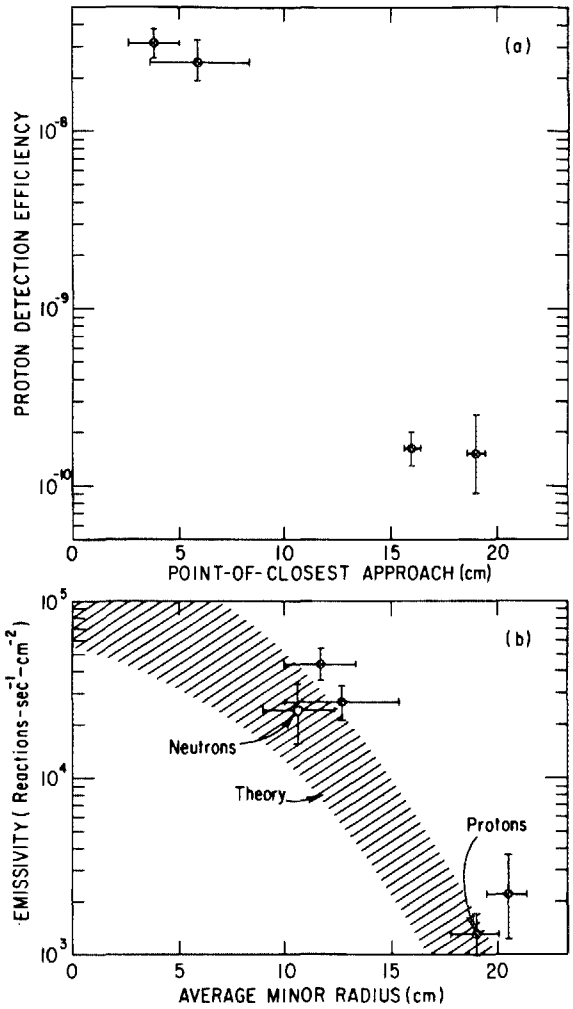

FIG. 17. (a) Proton detection efficiency vs point-of-closest approach to the magnetic axis during steady-state ohmic heating in PLT. $I_p = 470$ kA; $\bar{n}_e = 2.5\times10^{13}$ cm^{-3}; $T_e(0) = 1.7$ keV; $B_\phi = 31.3$ kG. The horizontal error bars indicate the change in the point-of-closest approach introduced by changing the detector pitch angle $\pm 3°$ and by varying the plasma current profile between $j \propto [1 - (r/a)^2]^{2\cdot6}$. The data are the average of 29 reproducible discharges. (b) Emissivity profile deduced using proton data. An approximate profile of the form $S = S_0 \exp[-(r/\alpha)^3]$, with $\alpha = 14.7 \pm 2.0$ cm, was fit to the raw data of (a) and of Fig. 5.21 of Ref. 21. Next, the proton detection efficiencies ϵ and the average minor radius $\langle r\rangle$ [Eq. (10)] were calculated using this approximate profile. The emissivity at $\langle r\rangle$ is then

$$S = C\exp[-(\langle r\rangle/\alpha)^3]/[\epsilon\tfrac{4}{3}\pi^2\Gamma(\tfrac{4}{3})R_0\alpha^2],$$

where C is the count rate at the detector, R_0 is the major radius of the emission (140 cm),[21] and $\Gamma(\frac{4}{3}) = 1.35$. The neutron datum was treated similarly, where now $\langle r\rangle$ is the volume-averaged emission radius, $\langle r\rangle \equiv \int rS(r)dV / \int S(r)dV$, and ϵ is the neutron detection efficiency.[32] The theoretical emissivity profile was deduced using neoclassical calculations[14] of the ion temperature profile, Thomson scattering measurements of the electron density, and analytical fits to the fusion reactivity.[33] The uncertainty reflects uncertainties in the deuterium depletion and in the role of terms that depend on the neutral density in the ion energy balance.

where $X_{\min}$ is the point-of-closest approach of the proton orbit to the magnetic axis. Defining the average radius of the emission $\langle r\rangle$ according to

$$\langle r\rangle = \int_{\text{swath}} rS\,dA \Big/ \int_{\text{swath}} S\,dA \tag{10}$$

and integrating Eqs. (9) and (10) numerically, we find that

typically $\langle r\rangle \simeq X_{\min} + 6$ cm [Fig. 18(a)]. As the point-of-closest approach $X_{\min}$ increases, the difference between the average radius $\langle r\rangle$ and the minimum radius decreases. Figure 18(b) examines the relationship between the measured proton flux and the emissivity at the average radius $\langle r\rangle$. To within 40%, the proton detection efficiency is linearly proportional to the emissivity at $\langle r\rangle$.

The preceding analysis suggests the following procedure for relating proton data from emission-profile detectors to the emissivity of the plasma: (1) Find the point-of-closest approach to the magnetic axis $X_{\min}$ using calculations of the accepted proton orbits. (2) Determine the scale length λ of the emissivity profile at $X_{\min}$ by varying the horizontal position of the plasma.[21] Alternatively, an estimate of the scale length can be obtained from the ratio of the fluxes measured by two adjacent detectors, $\lambda \simeq \Delta X_{\min}/\ln(\Phi_1/\Phi_2)$, where

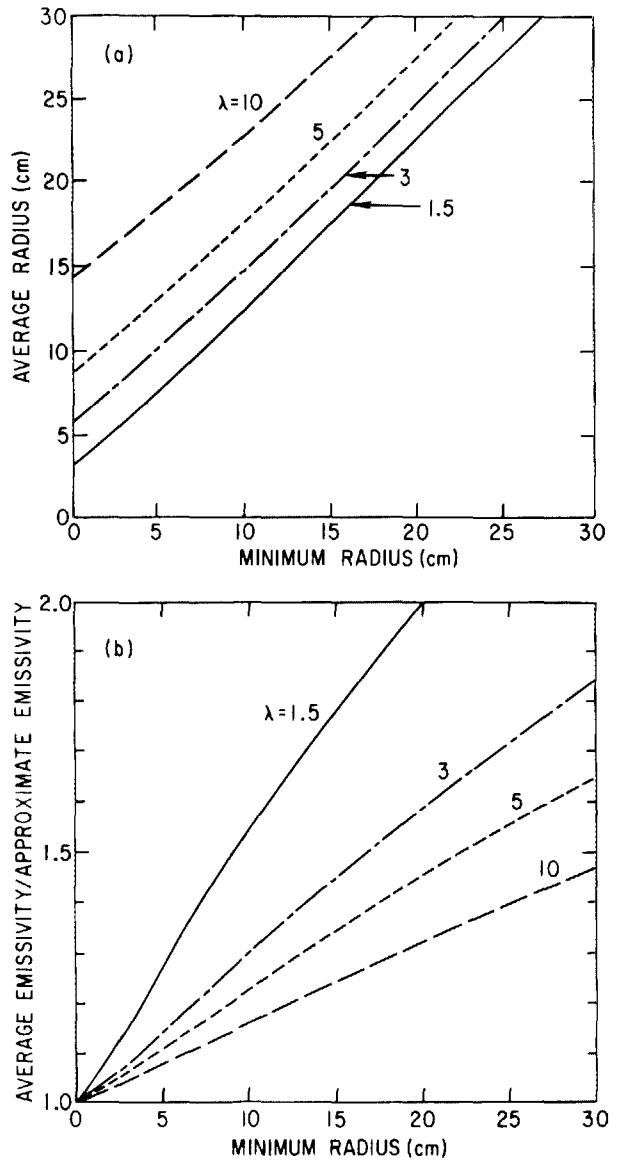

FIG. 18. (a) Average radius $\langle r\rangle$ [Eq. (10)] of the proton emission as a function of the point-of-closest approach for emission profiles of the form $S = \exp(-r/\lambda)$. (b) Normalized proton detection efficiency divided by the emissivity at $\langle r\rangle$ as a function of the point-of-closest approach for emission profiles of the form $S = \exp(-r/\lambda)$.

$\Delta X_{\min}$ is the spacing of the proton orbits at the midplane. (3) Use Fig. 18(a) to determine the average radius $\langle r\rangle$ of the measured proton emission. (4) Use Fig. 18(b) to find the relationship between the emissivity measured by the detector (average emissivity) and the emissivity at $\langle r\rangle$ (approximate emissivity). Adjust the proton data by this factor and a factor accounting for the differing drift velocities ($\int S\,dl$) of the proton orbits near $X_{\min}$ to obtain an approximation to the emissivity at $\langle r\rangle$. The relatively weak dependence of $\langle r\rangle$ [Fig. 18(a)] and of the correction factor of Fig. 18(b) on the scale length λ implies that, for an accuracy in determining λ of $\pm$ 25%, the emissivity deduced using this procedure is accurate to 10% with an accuracy in $\langle r\rangle$ of $\pm$ 2 cm. (5) Use this approximate emissivity profile as input into calculations employing the exact expression for proton detection efficiency [Eq. (3)]. Modify the profile until satisfactory agreement with experiment is obtained.

This procedure can be viewed as equivalent to an Abel inversion of data from chordal measurements of photons. As with photon chordal measurements, the accuracy of the inversion is enhanced by central peaking of the emissivity profile. The inversion of proton data differs from an Abel inversion because the proton "chords" are curves of nonuniform length.

The emissivity profile deduced from the data of Fig. 17(a) appears in Fig. 17(b). Because of the limited spatial information obtained in our experiments, the absolute accuracy of our emissivity measurement is comparable to the absolute accuracy of neutron measurements ($\pm$ 40%).[32] The data indicate that the relative accuracy of our measurements was typically 40% with a spatial resolution of $\pm$ 1–3 cm, which, for an accuracy in measuring the density of 25%, implies an accuracy in determining the ion temperature profile of about 20%.

In our experiments, only one detector (P118) was oriented to accept protons on near-stagnation orbits and the other detectors measured protons on orbits expected to be fairly insensitive to changes in poloidal field (Fig. 8). The sensitivity of proton orbits to changes in the poloidal field was studied by measuring the proton detection efficiency as a function of plasma current during steady-state operation (Fig. 19). As expected, the fluence at the detector (P118) that measures near-stagnation orbits fell strongly when the current was reduced. At lower poloidal field, the free-streaming contribution [Eq. (1)] to the proton motion becomes less important and the measured proton orbits become straighter (cf. Fig. 3). For P118, this results in a reduction in the proton fluence since the protons originate farther from the magnetic axis. For the other detectors, straighter proton orbits result in slightly higher detection efficiencies (Fig. 19). Detailed calculations[21] indicate that the data of Fig. 19 are consistent with the expected poloidal field dependence for our proton detectors.

IV. FUTURE PROTON DIAGNOSTICS

The observed accuracy of the 3-MeV proton ion temperature measurement is comparable to the accuracy previously achieved using active charge exchange in PLT.[14] Collimated 3-MeV proton measurements are potentially a

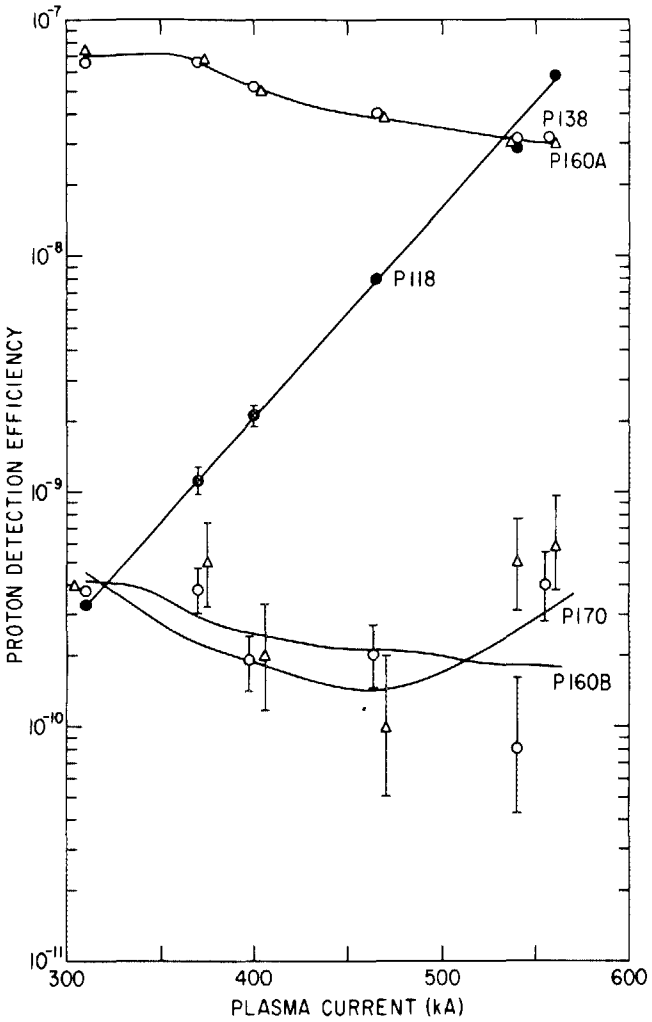

FIG. 19. Proton detection efficiency vs plasma current during steady-state ohmic operation in PLT ($B_\phi = 31.3$ kG; $\bar{n}_e = 2.5 \times 10^{13}$ cm^{-3}; deuterium). Each point is the average over 300 ms of the steady-state portion of 3–8 discharges. The curves are fits to the data.

very attractive technique for measuring the ion temperature profile. With reductions of detector noise and of proton scattering from the walls of the detector apparatus to improve the accuracy of the flux measurements, and with the ability to rotate the detectors in pitch angle to ensure the optimal orientations for emissivity measurements, quite accurate ($\pm$ 5% in T_i; $\pm$ 2 cm in R) determination of the deuterium ion temperature profile for $T_i \gtrsim 0.5$ keV appears possible. Unlike charge exchange, the proton measurements are easier at higher plasma density. Spectroscopic measurements of the Doppler broadening of visible atomic transitions have most often been performed in the outer part of the plasma,[14] where partially ionized intrinsic impurities reside. In the presence of a diagnostic neutral beam, measurements of the ion temperature profile via charge-exchange recombination spectroscopy of helium[15] and single-point ion temperature measurements using charge-exchange recombination radiation from hydrogen have been made,[34] but the accuracy achievable using these techniques appears inferior to that possible using 3-MeV protons. Ion temperatures also have been measured in tokamaks using detection of impurity x-ray lines[13] and by scattering fast ions,[35] but profile measurements using these approaches could be expensive. In summary, in plasmas where the deuterium distribution is believed to be Maxwellian, collimated 3-MeV proton detection promises to be a relatively accurate, inexpensive, passive, ion temperature diagnostic.

The principal limitation of the proton ion temperature diagnostic is relatively poor counting statistics when the ion temperature is below 1 keV. Other limitations are that the measurements can only be made in deuterium plasmas with low emission levels of hard x rays and of 14-MeV neutrons.

In plasmas with a nonthermal deuterium distribution, the emission profile diagnostic provides information on the spatial distribution of fast deuterons. Such measurements can be used to study the density profile of fast ions during wave heating or during neutral beam injection.[21]

Collimated measurements of 3-MeV protons also can be used to measure the poloidal field. These measurements are more difficult than the ion temperature measurements because they require more narrow and precise collimation. The technique requires simultaneous determination of the emission profile. Our initial experimental results from PLT confirm that, for a properly oriented detector, the flux does depend sensitively on the poloidal field. With the accuracy achieved in collimating our detectors (5° FWHM) and in measuring the proton flux (10%), it appears possible to measure the poloidal field at $r/a = 0.5\%$ to $\pm$ 25%. Soltwisch[3] has measured the poloidal field of the TEXTOR tokamak with better than 10% accuracy using Faraday rotation. The best resolution estimated to be achievable using proton measurements (assuming pitch-angle collimation of 1° FWHM and an accuracy in orienting the detector of better than $\pm$ 1°) is $\pm$ 5%.

Another possible approach to poloidal field measurements through 3-MeV proton detection is to construct a detector that can be rotated in pitch angle or, alternatively, to use a position-sensitive surface barrier detector in conjunction with a pinhole. The shape of the fluence as a function of pitch angle then provides a measure of the poloidal field distribution (Fig. 20). Compared to the use of stationary de-

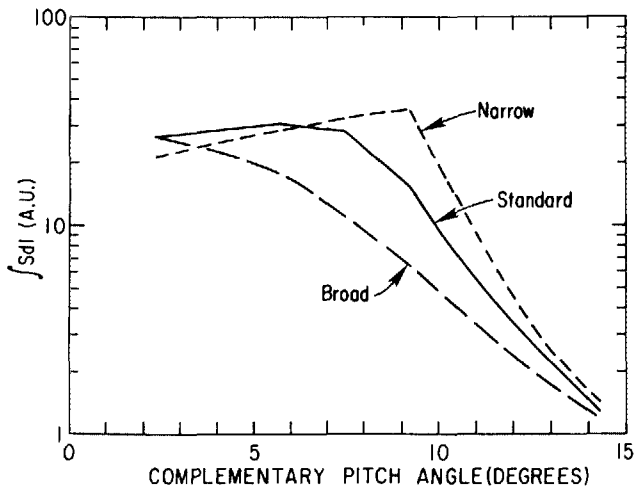

FIG. 20. Emission-weighted orbit length $\int S\, dl$ vs pitch angle for a detector positioned at $R = 108$ cm. The model current profiles are $j \propto [1 - (r/a)^2]^i$, with $i = 2$ (long dash), $i = 4$ (solid), and $i = 6$ (short dash). $S(r) \propto [1 - (r/a)^2]^9$.

tectors, this technique has the important advantage that the measurement is independent of the absolute calibration of the detector.

ACKNOWLEDGMENTS

We thank S. Cohen, S. von Goeler, R. Goldston, J. Lovberg, and W. Stodiek for helpful discussions, and J. Hosea and the PLT crew for their support of the experiments. R. Bell made the Thomson scattering measurements. G. Estepp did much of the design and fabrication of the proton detectors and assisted in the design and construction of the apparatus for their calibration. J. Hosea suggested the use of the magnetic loops. R. Chrien wrote the first version of the detection efficiency computer code.

This work was supported by U. S. Department of Energy Contract No. DE-AC02-76-CHO-3073.

APPENDIX: CALCULATION OF DETECTION EFFICIENCY

To evaluate Eq. (3) numerically, the proton orbit is first calculated and then the integral $\int d\Omega\ T(\Omega)\int S\,dl$ is summed.

The orbit of a charged particle in a magnetic field is given by the Lorentz force law. In calculations involving the orbits of thermal particles it is often impractical to work with the full gyro-orbit because of the disparate time scales between cyclotron motion and drift-orbit motion but, for fusion products, the ratios of orbit size to system size and vertical drift velocity to particle velocity are large enough that it is practical to integrate the Lorentz force law directly. Exploiting the microscopic reversibility of particle motion, the code calculates the time-reversed orbit of a particle that arrives at the detector position with the desired "initial" velocity by integrating the Lorentz force law (a second-order ordinary differential equation) using a package equation solver (usually, the IMSL routine DVERK; the EXTINT routine[36] has also been used and gave similar results). Cylindrical coordinates (R,ϕ,z) are employed. The magnetic field used in the calculation is the lowest-order approximation (in an inverse-aspect ratio expansion) to the actual axisymmetric tokamak field[37]:

$$\begin{aligned} B_\phi &= B_0R_0/R, \\ B_R &= -\sin\theta B_\theta(r)R_0/R, \\ B_z &= \cos\theta B_\theta(r)R_0/R. \end{aligned} \tag{A1}$$

Here, r and θ are the coordinates of concentric circular flux surfaces:

$$\begin{aligned} r &= \sqrt{z^2+(R-R_0)^2}, \\ \theta &= \sin^{-1}(z/r). \end{aligned} \tag{A2}$$

The poloidal field B_θ is approximated by the field produced by a longitudinal current $j\propto[1-(r/a)^2]^i$ in a cylinder:

$$B_\theta = \frac{\mu_0 I}{2\pi r}\{1-[1-(r/a)^2]^{i+1}\}. \tag{A3}$$

Outside the limiter radius a, the poloidal field is assumed to fall off inversely with minor radius.

It should be noted that the aspect ratio $r/R\sim0.3$ is not a particularly good expansion parameter for PLT and that the model magnetic field [Eq. (A1)] is not divergenceless for finite i. For PLT, the vertical equilibrium field $B_\perp$ is fairly large compared to the poloidal field ($B_\perp\sim0.3B_\theta$) and the Shafranov shift is typically 3–5 cm.

In calculations of detection efficiency, the time-reversed orbit is stopped when it strikes the vacuum vessel wall.

The calculation of proton orbits was checked by comparing the computed Larmor radius and drift velocity with analytical estimates of these quantities.

Equation (3) is then evaluated as follows: The detector collimation is approximated by the transparency of a two-dimensional slot using Eq. (4). The integral over Ω is broken up into an odd number of intervals in each of the two dimensions. For each angle Ω, the time-reversed orbit of a proton that strikes the detector position with that velocity is calculated. The proton orbit is broken into segments (typically 2 cm) and the emission-weighted orbit length $\int S\,dl$ is computed for that orbit using an analytical approximation to the emission profile. The weighted orbit length is then weighted by the transparency $T(\Omega)$ and added to the sum to obtain an approximation to $\int d\Omega\ T(\Omega)\int S\,dl$.

The accuracy of the calculation was checked by replacing the proton orbits with straight orbits and numerically calculating the *photon* detection efficiency. The result agreed to within 10^{-4} with analytical evaluation[21] of the detection efficiency.

[1]Equipe TFR, Nucl. Fusion **18**, 658 (1978).
[2]W. Kunz, Nucl. Fusion **18**, 1729 (1978).
[3]H. Soltwisch, in Proceedings of the EPS, Aachen, 1983, Vol. 7D, Part 1, p. 123; H. Soltwisch and Equipe TFR, Infrared Phys. **21**, 287 (1981).
[4]D. P. Hutchinson *et al.*, Nucl. Fusion **21**, 1535 (1981); C. H. Ma *et al.*, Int. J. Infrared Millimeter Waves **3**, 263 (1982).
[5]J. Fujita and K. McCormick, in *Sixth European Conference on Contr. Fusion and Plasma Physics* (Moscow, 1973), Vol. I, p. 191.
[6]M. J. Forrest *et al.*, Culham Laboratory Report CLM-P499, 1977.
[7]R. J. Goldston, Phys. Fluids **21**, 2346 (1978).
[8]A. de Chambrier *et al.*, Phys. Lett. A **92**, 279 (1982).
[9]S. von Goeler *et al.*, Phys. Rev. Lett. **33**, 1201 (1974).
[10]V. S. Mukhovatov and V. D. Shafranov, Nucl. Fusion **11**, 605 (1971).
[11]For example, C. F. Barnett and J. A. Ray, Nucl. Fusion **12**, 65 (1972).
[12]L. A. Artsimovich, Sov. Phys. JETP **34**, 306 (1972).
[13]M. Bitter *et al.*, Phys. Rev. Lett. **42**, 304 (1979).
[14]M. Brusati *et al.*, Nucl. Fusion **18**, 1205 (1978).
[15]R. J. Fonck, D. S. Darrow, and K. P. Jaehnig, Phys. Rev. A **29**, 3288 (1984).
[16]V. V. Afrosimov, M. P. Petrov, and V. A. Sadovnikov, Sov. Phys. JETP Lett. **18**, 300 (1973).
[17]J. D. Strachan *et al.*, Phys. Lett. A **66**, 295 (1978).
[18]J. J. Schuss *et al.*, Nucl. Fusion **21**, 427 (1981).
[19]R. E. Chrien, R. Kaita, and J. D. Strachan, Nucl. Fusion **23**, 1399 (1983).
[20]F. H. Tenney, Princeton Plasma Physics Laboratory Report MATT-1132, 1975.
[21]W. W. Heidbrink, Ph.D. thesis, Princeton University, 1984.
[22]J. A. Rome *et al.*, Nucl. Fusion **16**, 55 (1976).
[23]R. E. Chrien and J. D. Strachan, Phys. Fluids **26**, 1953 (1983).
[24]H. Eubank *et al.*, in Proceedings of the Third Varenna-Grenoble International Symposium, 1982, Vol. 1, p. 15.
[25]W. W. Heidbrink, R. Hay, and J. D. Strachan, Phys. Rev. Lett. **53**, 1905 (1984).
[26]An alternative derivation of the expression for proton detection efficiency appears in Ref. 23.
[27]H. Goldstein, *Classical Mechanics* (Addison-Wesley, Reading, MA, 1950), p. 266.

[28]*Ion Implanation Techniques*, edited by H. Ryssel and H. Glawischnig (Springer–Verlag, New York, 1982), p. 291.
[29]W. W. Heidbrink, Nucl. Fusion **24**, 636 (1984).
[30]W. W. Heidbrink, R. E. Chrien, and J. D. Strachan, Nucl. Fusion **23**, 917 (1983).
[31]H. H. Anderson and J. F. Zigler, *The Stopping and Ranges of Ions in Matter, Vol. 3* (Pergamon, New York, 1977).
[32]G. Zankl, J. D. Strachan, R. Lewis, W. Pettus, and J. Schmotzer, Nucl. Instrum. Methods **185**, 321 (1981).
[33]G. H. Miley, H. Towner, and N. Ivich, Report No. COO-2218-17, University of Illinois, 1974.
[34]G. A. Cottrell, Nucl. Fusion **23**, 1689 (1983).
[35]E. L. Berezovskii *et al.*, Sov. J. Plasma Phys. **6**, 760 (1980).
[36]J. Boris and N. Winsor, Princeton Plasma Physics Laboratory Report PPPL-652, 1970.
[37]G. Knorr, Phys. Fluids **8**, 1334 (1965).